Thesis for the degree of Doctor of Philosophy

Turbulent and neoclassical transport in tokamak plasmas

István Pusztai

CHALMERS

Nuclear Engineering
Department of Applied Physics
Chalmers University of Technology
Göteborg, Sweden, 2011

Turbulent and neoclassical transport in tokamak plasmas
István Pusztai

ISBN 978-91-7385-581-5
Doktorsavhandlingar vid Chalmers tekniska högskola
Ny serie nr 3262
ISSN 0346-718X

Department of Applied Physics
Chalmers University of Technology
SE–412 96 Göteborg
Sweden
Telephone +46–(0)31–772 10 00

Printed in Sweden by
Reproservice
Chalmers Tekniska Högskola
Göteborg, Sweden, 2011

Turbulent and neoclassical transport in tokamak plasmas

István Pusztai
Department of Applied Physics
Chalmers University of Technology

Abstract

One of the greatest challenges of thermonuclear fusion is to understand, predict and to some extent control particle and energy transport in fusion plasmas. In the present thesis we consider theoretical and experimental aspects of collisional and turbulent transport in tokamak plasmas.

First the collisionality dependence of quasilinear particle flux due to ion temperature gradient (ITG) and trapped electron modes is investigated. A semi-analytical gyrokinetic model of electrostatic microinstabilities is developed and used to study various parametric dependences of ITG stability thresholds and quasilinear particle and energy fluxes, focusing on the effect of collisions.

Then corrections to the neoclassical plateau regime transport in transport barriers are calculated. It is found that the ion temperature gradient drive of the bootstrap current can be enhanced significantly, and the ion heat diffusivity and the poloidal flow of trace impurities are also modified in the presence of strong radial electric fields.

Furthermore, we investigate the characteristics of microinstabilities in electron cyclotron heated and ohmic discharges in the T10 tokamak using linear gyrokinetic simulations, aiming to find insights into the effect of auxiliary heating on the transport, with special emphasis on impurity peaking.

The effect of primary ion species of differing charge and mass on instabilities and transport is studied through linear and nonlinear gyrokinetic simulations. We perform transport analysis of three balanced neutral beam injection discharges from the DIII-D tokamak which have different main ion species (deuterium, hydrogen and helium).

Finally the magnitude and characteristics of the error in alkali beam emission spectroscopy density profile measurements due to finite beam width are analyzed and a deconvolution based correction algorithm is introduced.

Keywords: thermonuclear fusion, tokamaks, microinstabilities, turbulent transport, neoclassical transport, transport barriers, impurity transport, isotope effect, transport analysis

Publications

[A] T. Fülöp, I. Pusztai, and P. Helander "Collisionality dependence of the quasilinear flux due to microinstabilities", Phys. Plasmas **15**, 072308 (2008).

[B] I. Pusztai, T. Fülöp, J. Candy, and R. J. Hastie, "Collisional model of quasilinear transport driven by toroidal electrostatic ion temperature gradient modes", Phys. Plasmas **16**, 072307 (2009).

[C] I. Pusztai and P. J. Catto, "Neoclassical plateau regime transport in a tokamak pedestal", Plasma Phys. Control. Fusion **52**, 075016 (2010).

[D] I. Pusztai, S. Moradi, T. Fülöp, and N. Timchenko, "Characteristics of microinstabilities in electron cyclotron and ohmic heated discharges", Phys. Plasmas **18**, 082506 (2011).

[E] I. Pusztai, J. Candy, and P. Gohil, "Isotope mass and charge effects in tokamak plasmas", accepted for publication in Phys. Plasmas.

[F] I. Pusztai, G. Pokol, D. Dunai, D. Réfy, G. Pór, G. Anda, S. Zoletnik, and J. Schweinzer, "Deconvolution-based correction of alkali beam emission spectroscopy density profile measurements", Rev. Sci. Instrum. **80**, 083502 (2009).

Other contributions (not included in the thesis)

[G] P. J. Catto, G. Kagan, M. Landreman, and I. Pusztai, "A unified treatment of kinetic effects in a tokamak pedestal", Plasma Phys. Control. Fusion **53**, 054004 (2011).

[H] T. Fülöp, S. Braun, and I. Pusztai, "Impurity transport driven by ion temperature gradient turbulence in tokamak plasmas", Phys. Plasmas **17**, 062501 (2010).

[I] S. Moradi, T. Fülöp, A. Mollén, and I. Pusztai, "A possible mechanism responsible for generating impurity outward flow under radio frequency heating ", Plasma Phys. Control. Fusion **53**, 115008 (2011).

[J] I. Pusztai, J. Candy, P. Gohil, and E. A. Belli, "Isotope mass and charge effects in tokamak plasmas", Proceedings of the 38th EPS Conference on Plasma Physics, P-5.110 (2011).

[K] T. Fülöp, S. Moradi, A. Mollén, and I. Pusztai, "The role of poloidal asymmetries in impurity transport", Proceedings of the 38th EPS Conference on Plasma Physics, P-2.114 (2011).

[L] D. Guszejnov, G. I. Pokol, I. Pusztai, and D. Réfy, "Applications of the RENATE beam emission spectroscopy simulator", Proceedings of the 38th EPS Conference on Plasma Physics, P-2.054 (2011).

[M] I. Pusztai and P. J. Catto, "Neoclassical plateau regime transport in a tokamak pedestal", Proceedings of the 37th EPS Conference on Plasma Physics, ECA Vol.**34A**, P-1.1082 (2010).

[N] T. Fülöp, S. Braun, and I. Pusztai, "Impurity transport driven by electrostatic turbulence in tokamak plasmas", Proceedings of the 37th EPS Conference on Plasma Physics, ECA Vol.**34A**, P-1.1028 (2010).

[O] T. Fülöp, S. Braun, and I. Pusztai, "Impurity transport driven by electrostatic turbulence in tokamak plasmas", Proceedings of 23rd IAEA Fusion Energy Conference, pp. THC/P4-09 (2010).

[P] S. Kálvin, G. Anda, D. Dunai, G. Petravich, S. Zoletnik, G. Pokol, B. Játékos, I. Pusztai, and D. Réfy, "Reconstruction of plasma

edge density profile from Lithium beam data using statistical analysis", Proceedings of the 36th EPS Conference on Plasma Physics, ECA Vol.**33E**, P-5.211 (2009).

[Q] I. Pusztai, T. Fülöp, and P. Helander, "On the quasilinear transport fluxes driven by microinstabilities in tokamaks", Proceedings of the 35th EPS Conference on Plasma Physics, ECA Vol.**32D**, P-1.032 (2008).

[R] T. Fülöp, I. Pusztai, and P. Helander, "Quasilinear transport fluxes driven by electrostatic microinstabilities in tokamaks", Proceedings of 22nd IAEA Fusion Energy Conference, pp. TH/P8-28. (2008).

[S] I. Pusztai, D. Dunai, G. Pokol, G. Pór, J. Schweinzer, and S. Zoletnik, "Capabilities of alkali Beam Emission Spectroscopy for density profile and fluctuation measurements", Proceedings of the 34th EPS Conference on Plasma Physics, ECA Vol.**31F**, P-2.137 (2007).

Contents

Acknowledgments

First of all I would like to thank my supervisor, Tünde Fülöp with her kindness, brilliance and exceptional intuitiveness, for her support, encouragement and valuable guidance in research and in other areas of life.

I am very grateful to my MSc supervisor, Gergő Pokol, who started me on this path, for his support, guide and friendship.

Special thanks go to my temporary or external supervisors: I would like to thank Jeff Candy with his explanatory talent, for the fruitful discussions. I am indebted to Peter Catto who always found the time for sharing his sharp insights to physical problems. And finally, the help and instructive guidance of Per Helander is greatly acknowledged. I am really thankful for the Fusion Theory group at General Atomics and the Plasma Science and Fusion Center at MIT for supporting my visits and for their hospitality.

I am very grateful to all my colleagues at Nuclear Engineering for providing a welcoming stimulating atmosphere, especially to professor Imre Pázsit and to Albert, Geri and Sara from the Fusion Theory group.

I will always remember the "good old days" at the group of Nonlinear Electrodynamics, where I am thankful for professors Mietek Lisak and Dan Anderson, and the graduate students Robert, Tobias and Joel for providing an inspiring atmosphere.

I would also like to thank all my coauthors and collaborators for their help.

But above all, I owe my warmest gratitude to my little family; my wife Renáta, for her patience, encouragement and love, and my daughter, Isgerdur.

Chapter 1

Introduction

The ever increasing energy demand of humanity, our finite non-renewable resources and the threatening extent of environmental pollution establish the need for a new, clean and large-scale energy source. One of the most promising candidates for this purpose is controlled thermonuclear fusion which has been an intensely explored area for more than half a century.

Fusion utilizes the energy that is released as two light nuclei fuse together, and provides one of the main energy sources of the Universe. The reaction between the positively charged nuclei is obstructed by their Coulomb repulsion, so that bringing even the most feasible fusion process [$\mathrm{D} + \mathrm{T} \rightarrow {}^4\mathrm{He}$ (3.5 MeV) + n (14.1 MeV)] to effect with reasonable efficiency (at achievable density) requires a temperature of $\sim 10^8$ K, which implies that in laboratory conditions the fusion fuel has to be confined by some special means. Fortunately, the extremely high temperatures giving rise to the difficulties of confinement also provide a possible solution, since the matter is then in an almost fully ionized, plasma state which can be confined with a magnetic field.

As a consequence of the Poincaré–Hopf theorem [1], the only topology in three dimensions which has non-vanishing continuous tangent vector field is the torus. Accordingly, in order to prevent end losses, the most successful magnetic confinement fusion devices, the stellarator [2] and the tokamak [3] have toroidal magnetic geometry; i.e. their magnetic field lines trace out nested toroidal surfaces. The tokamak is axisymmetric and the twist of its magnetic field, which is necessary for magnetohydrodynamic stability purposes, is maintained by a current driven inductively in the plasma. According to its relative simplic-

ity, both its theory and technology have developed relatively rapidly, so that the experimentally achieved value of the *fusion triple product* $n_i T_i \tau_E$, which is the main indicator of fusion performance, has doubled approximately every second year since the mid-1950's (n_i and T_i are the ion density and temperature and τ_E is the characteristic time of the energy confinement).

Since the magnetic field of a stellarator is generated by external coils, its operation does not rely on inductively driven toroidal current, that makes a continuous operation possible, which is clearly desirable in reactors. Also, in contrast to tokamaks, the stellarator lacks current induced instabilities and a hard operational limit on plasma density (Greenwald limit [4]). However, due to the lack of toroidal symmetry, the radial confinement of plasma particles is not guaranteed; its magnetic geometry has to be optimized to avoid drift losses. Especially the confinement of high energy ions is an issue in stellarators. The helical structure of the magnetic field is produced by a complex magnetic coil system. Since the sufficient computational capacity for the optimized design of such complicated, inherently three-dimensional system has been achieved only in the recent years, the stellarator has lagged behind the tokamak concept, in terms of confinement properties and number of experiments.

On the road towards controlled thermonuclear fusion it was a notable event when, in 1997, the largest current fusion experiment, JET (Joint European Torus) produced 16 MW of fusion power – 65% of the input power [5]. The "next step" will be an even bigger tokamak experiment, ITER, which is under construction at the present time. Its goal is to demonstrate the technical feasibility of fusion energy production by generating 500 MW fusion power from 50 MW input power [6]. Considerable knowledge on the behavior of fusion plasmas has been accumulated in the recent decades that enabled the design of this experimental fusion reactor. However, most of our predictions regarding the performance of ITER are based on extrapolations using empirical scaling laws [7]. Even today we lack a comprehensive and accurate description of the transport processes in fusion plasmas due to the complexity of the problem.

For efficient fusion energy production the energy transport through the magnetic surfaces should be minimized, and at the same time, to maintain the "burning" plasma, the particle transport has to be kept under control. In addition to the ubiquitous but tolerable level of diffusive collisional transport (which is called "neoclassical" transport), the major part of the transport is due to convective fluxes associated with

plasma turbulence. This turbulence is driven by various kinds of small-scale, low-frequency unstable modes, microinstabilities, due to density or temperature gradients [8]. Even hydrodynamic turbulence is a complex unresolved problem, and considering several fluid species coupled through electromagnetic, friction and energy exchange effects, it is not surprising that there is no general theory of plasma turbulence. Understanding and accurately predicting the turbulent transport is one of the most challenging theoretical issues of magnetic confinement fusion.

The complexity of the problem – nonlinear coupling between the different modes, turbulent cascades through the different spatial scales, nonlinear self-regulation – almost makes analytical treatment impossible, although there are methods such as renormalization [9], quasi-linear [10] and mixing-length approaches that have been used – with limited success. It seems that one has to resort to nonlinear kinetic or fluid simulations to obtain an overall picture of turbulent transport; accordingly, several kinetic and fluid simulation codes have been developed in the recent decades. Nevertheless, to understand the underlying physical mechanisms and to ease the interpretation of simulation results it is rather important to develop reduced models and investigate the properties and different parametric dependences of microinstabilities.

The drive of turbulence in the plasma core in a conventional tokamak, is typically dominated by toroidal ion temperature gradient (ITG) modes [11–13] and in certain cases trapped electron (TE) [14–16] modes, but the electron temperature gradient (ETG) mode [17, 18], and micro-tearing modes can also play an important role [19]. In the core, the level of the density and temperature fluctuations is only a few percent of the corresponding equilibrium quantities, while, in the plasma edge and scrape-off layer (SOL) they can be comparable. In the latter, outer plasma regions mainly electrostatic fluid instabilities – driven by gradients in pressure, current or resistivity – dominate the turbulence.

To achieve reactor relevant conditions it is essential to understand, reliably predict and – to some extent – control turbulent transport. It was discovered that by applying sufficiently high auxiliary heating power, a rapid spontaneous transition to an improved confinement mode – the so called high confinement- or H-mode [20] – can be obtained, which involves the formation of a transport barrier at the plasma edge, the so called pedestal. In the H-mode pedestal or in artificially induced internal transport barriers [21] the turbulent transport is strongly reduced, in particular the ion energy transport can be on the level of the collisional

transport. Long wavelength neoclassical sheared flows within the flux surfaces play an important role in the suppression of turbulence. For these reasons it is also important to have an accurate knowledge of neoclassical transport.

Due to the reduced transport in the edge transport barrier, strong pressure and current gradients can build up, that can destabilize magnetohydrodynamic (MHD) instabilities, leading to abrupt, quasi-periodic, burst-like ejection of a considerable part of the energy stored in the transport barrier region. These instabilities are called ELMs (edge localized modes) and can cause intolerable damage in the plasma limiting elements or at least contribute to their deterioration, but on the other hand they can be useful for helium ash removal [22]. In toroidal geometry density and temperature gradients drive a non-inductive current, the "bootstrap current", which plays a crucial role in reactor relevant operation by reducing the need for inductive current drive. This current, which can be considered as one of the most important predictions of neoclassical theory, can destabilize current-driven instabilities, in particular in the plasma edge it contributes to the drive of ELMs [23].

For the deeper understanding of these complex phenomena determining the overall transport of heat and particles, strong interaction between theoretical and experimental work is needed. A routinely applied method for electron density profiles and density fluctuation measurement at the SOL, edge, or outer core regions is beam emission spectroscopy (BES) [24,25]. It is based on the observation of a high energy collimated neutral beam injected into the plasma for heating or purely diagnostic purposes. The photons emitted in the spontaneous de-excitation of collisionally excited beam atoms carry information on the distribution of plasma parameters.

The collisions also lead to ionization of the beam atoms, resulting in beam attenuation, which usually restricts the diagnostic to the outer plasma regions. Accordingly, it is well suited for turbulence measurements there, as well as for the investigation of equilibrium or fluctuation driven flows in the edge, together with ELMs, geodesic acoustic modes [26] or other transient phenomena affecting the transport.

The remainder of the thesis is organized as follows. In Chapter 2 we introduce basic theoretical concepts that are used in the kinetic modeling of transport phenomena in magnetic confinement fusion devices. In particular we introduce magnetized plasmas and touch upon the particle motion in tokamak geometry before we give an introduction to

gyro-averaged kinetic theories. In Chapter 3, after a short introduction to collisional transport in general we restrict our attention to neoclassical transport and the relevant kinetic description, the drift kinetic formalism. We give an overview of the different collisionality regimes and sketch the physics of the bootstrap current, and finally discuss the issues of the neoclassical formalism in transport barriers. In Chapter 4 we start with discussing important tools to study microinstabilities and turbulence: the gyrokinetic theory and the ballooning formalism. Then the turbulent and quasilinear fluxes are discussed, before an overview of the characteristics of the two most important microinstabilities, the ion temperature gradient and trapped electron modes is given. A separate section is dedicated to the role of collisions in anomalous transport from both experimental and theoretical perspectives. Chapter 4 is closed by a short discussion of nonlinear simulations. Chapter 5 concerns turbulence and density profile measurements with beam emission spectroscopy. We close by summarizing the included papers in Chapter 6.

Chapter 2

Basic concepts in the transport of magnetized plasmas

In this chapter we provide a brief overview of the physical and theoretical concepts appearing in the field of transport theory of magnetized plasmas to be used in the following parts of the thesis, however we do not intend to reproduce the derivation of basic plasma physics results. Another aim of this section is to delineate the scope and limitations of the models to be presented.

2.1 Magnetized fusion plasmas

In the thesis the physics of fusion plasmas is studied. Plasma is a partially or fully ionized matter. We focus on fully ionized plasmas that are relevant in the core of fusion devices. The plasma consists of unbounded electrons and ions and in the applications of interest these can be considered as classical (i.e. not quantum) objects, that is a very good approximation for energies ($\sim$ keV) and densities ($\sim 10^{20}\mathrm{m}^{-3}$) typical in magnetic confinement fusion.

A complete definition of plasmas involves also spatial and time scales. The plasma is *quasi-neutral*, that is, in any macroscopic volume the quantity $(n_e - \sum_i Z_i n_i)/n_e \ll 1$, where $n_{e(i)}$ is the density of electrons (ions) and the sum runs over all the ion species with the charge Z_i. This approximate condition can be shown to be valid only for length scales larger than the *Debye length* $\lambda_D = \sqrt{\epsilon_0 T_e / e^2 n_e}$ (where T_e is the electron

temperature), and time scales longer than the inverse plasma frequency $1/\omega_{pe} = \sqrt{m_e\epsilon_0/n_e e^2}$. With other words, the plasma does not allow macroscopic charge separation. However, it does not imply that there can be no electrostatic fields present in plasmas, because extremely small charge separation can give rise to considerable electric fields.

The ion composition in fusion reactors is dominated by the fuel ions, namely deuterium and tritium. However, apart from a limited number of D-T experiments, the vast majority of the experimental discharges operate with a single species (mostly deuterium). Accordingly, the theoretical work done in transport theory usually considers a single hydrogenic species, which we refer to as the main species. Other ion species are also present in the plasma – preferably in smaller quantities; these *impurities* can come from the plasma facing components interacting with the plasma, and the helium "ash" of the fusion reactions also constitutes as impurity. For plasmas with several ion species it is useful to introduce the effective ion charge $Z_{\text{eff}} = \left(\sum_i n_i Z_i^2\right)/n_e$, which appears in several contexts in fusion plasma physics (for instance in the field of collisional transport), and is an important measure of the purity of plasmas.

The plasmas to be considered are magnetized in the sense that the collision frequency ν_a for a species a is much smaller than the cyclotron frequency $\nu_a \ll \Omega_a$ ($\Omega_a = e_a B/m_a$ with the charge and mass of the species e_a and m_a, and the magnetic field strength B), and that the typical length scale on which the equilibrium plasma parameters vary, L, is much larger than the ion Larmor radius $\rho_i \ll L$ ($\rho_i = v_\perp/\Omega_i$, where $v_\perp$ is the magnitude of the velocity component perpendicular to the magnetic field. The scale length of a plasma parameter X is usually defined as $L_X = -|\nabla \ln X|^{-1}$). The smallness of the parameter $\delta = \rho_i/L$ provides the basis of virtually the whole field of transport theory of fusion plasmas operating with gyro-averaged kinetic equations kept through certain order in δ.

2.2 Magnetic geometry and particle motion

In a homogeneous magnetic field the particle motion can be conveniently decomposed to a gyration perpendicular to the magnetic field lines with the cyclotron frequency (Larmor motion), and a free motion along the magnetic field line. Thus the particle trajectory traces out a helix with the position of its *guiding center* $\mathbf{R} = \mathbf{r} - (\mathbf{b} \times \mathbf{v})/\Omega_a$, where $\mathbf{r}$ is the actual position and $\mathbf{v}$ is the velocity of the particle, $\mathbf{b} = \mathbf{B}/B$ is the

unit vector in the direction of the magnetic field $\mathbf{B}$. In this simple configuration the velocity of the guiding center $\dot{\mathbf{R}}$ is $\mathbf{v}_\parallel = \mathbf{b}v_\parallel$, where the parallel velocity is $v_\parallel = \mathbf{b} \cdot \mathbf{v}$.

If the magnetic field has a spatial variation and/or there is an electrostatic field present, the motion of the guiding center is more complicated: In the parallel direction the particle can be accelerated by the parallel component of the electric field and it is also affected by the magnetic mirror force acting in the direction opposite to the gradient of the field strength. The magnitude of the mirror force is $\mu\nabla_\parallel B$, where $\mu = mv_\perp^2/(2B)$ is the magnetic moment of the gyrating particle with $v_\perp$ the magnitude of the perpendicular velocity $\mathbf{v}_\perp = \mathbf{v} - \mathbf{v}_\parallel$. Perpendicularly to the magnetic field the guiding center drifts with a velocity

$$\mathbf{v}_d = \dot{\mathbf{R}}_\perp = \frac{\mathbf{E} \times \mathbf{B}}{B^2} + \frac{v_\perp^2}{2\Omega}\mathbf{b} \times \nabla \ln B + \frac{v_\parallel^2}{\Omega}\mathbf{b} \times \boldsymbol{\kappa}. \tag{2.1}$$

The first term in the right hand side of Eq. (2.1) is called the $\mathbf{E} \times \mathbf{B}$ drift, and it is independent of the charge or mass of the particle species. The direction of the other two terms arising due to inhomogeneities in the magnetic field, called the grad-B drift and the curvature drift respectively, depend on the sign of the particle charge. We introduced the curvature vector of the magnetic field $\boldsymbol{\kappa} = -\mathbf{b} \times (\nabla \times \mathbf{b})$ in the curvature drift term which, in the limit of low normalized pressure $\beta = 2\mu_0 p/B^2$ (μ_0 is the vacuum permeability), can be approximated as $\boldsymbol{\kappa} \approx \mathbf{b} \times \nabla \ln B$ to get a similar form to the grad-B drift. Then the magnetic drift velocity $\mathbf{v}_D$ can be written simply as

$$\mathbf{v}_D = \frac{1}{\Omega}\left(\frac{v_\perp^2}{2} + v_\parallel^2\right)\mathbf{b} \times \nabla \ln B. \tag{2.2}$$

The derivation of the drift velocities (or more generally, the "guiding center" picture of particle motion) assumes that $|\mathbf{v}_d| \ll |\mathbf{v}|$, which is posteriorly justified for the cases we study. It implies that the motion of an "average" particle along the magnetic field line is much faster than its drift across the field lines; this is one of the reasons why the geometry of magnetic field lines plays a crucial role in transport theory. The field lines in toroidally symmetric configurations trace out surfaces, which we call magnetic surfaces or *flux surfaces*. In plasmas in magnetohydrodynamic equilibrium (which we shall consider), the radial pressure gradient is balanced by the $\mathbf{J} \times \mathbf{B}$ force, where $\mathbf{J}$ is the plasma current density. It follows from the MHD momentum equation $\mathbf{J} \times \mathbf{B} = \nabla p$,

that $\mathbf{B} \cdot \nabla p = 0 = \mathbf{J} \cdot \nabla p$, which means that currents flow within the flux surfaces that also coincide with the surfaces of constant pressure. As we will see not just the total kinetic pressure, but the densities and temperatures of each species separately are also approximately constants on flux surfaces. However, fast toroidal rotation of heavy impurity ions and other physical phenomena can cause significant poloidal asymmetries.

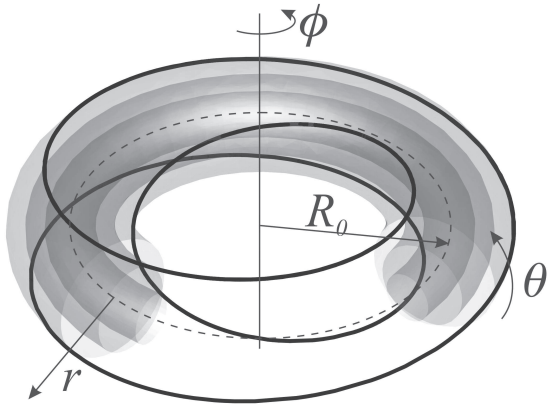

Figure 2.1: Toroidal geometry. r denotes the radial coordinate, ϕ and θ are the toroidal and the poloidal angles, respectively, and R_0 is the major radius of the torus. Three nested flux surfaces are indicated, and the thick line represents a magnetic field line in the $q = 3$ magnetic surface.

Due to the importance of the flux surfaces, the usual "radial" coordinate is chosen to be a *flux function*, i.e. a quantity which is constant on a flux surface, and monotonously increasing between the *magnetic axis* (the innermost flux surface degenerated to a line) and the *last closed flux surface* (LCFS) (the last magnetic surface whose field lines do not go through any plasma facing component). It can be the poloidal flux Ψ, which is – apart from a constant multiplier – the magnetic flux through a surface between the magnetic axis and an arbitrary line lying in a flux surface encircling the torus once toroidally while not making a poloidal turn. Another convenient choice is the toroidal flux Ψ_T, that is the magnetic flux trough a loop lying in a flux surface making one poloidal loop. To get a radial coordinate with length dimension, sometimes $r_\Psi \sim \sqrt{\Psi_T / B_0}$ is used with some reference field B_0.

Since both Ψ and Ψ_T are (radially monotonously increasing) flux functions they can be written as functions of each other, such as $\Psi_T(\Psi)$.

The dimensionless function $q(\Psi) = d\Psi_T(\Psi)/d\Psi$, the so called *safety factor*, is a measure of the helical "twistedness" of the field lines; it means – in a flux surface average sense – the number of toroidal turns needed to encircle the flux surface poloidally when following a magnetic field line. In tokamaks q usually (but not necessarily) monotonically increases radially from a value around 1; its radial logarithmic derivative $s = r(d\ln q/dr)$ is called the magnetic shear. In Fig. 2.1 a magnetic field line in the $q = 3$ flux surface is shown together with a set of toroidal coordinates.

In toroidally symmetric configurations the magnetic field can be conveniently expressed as

$$\mathbf{B} = I(\Psi)\nabla\varphi + \nabla\varphi \times \nabla\Psi, \tag{2.3}$$

where the first term is the toroidal component of the field B_t with $I = RB_t$, the second term is the poloidal field B_p, and φ denotes the toroidal angle. In tokamaks the ratio of the poloidal and toroidal components of the magnetic field is mostly much larger than unity and can be approximated as $B_t/B_p \approx qR/r$, with R and r being the major and minor radii, respectively, and their ratio R/r is called the *aspect ratio*.

From $B_p/B_t \ll 1$ it follows that Eq. (2.2) describes a drift dominantly in the vertical direction. Therefore a guiding center moving along the field line drifts off from a given flux surface. For purely toroidal field it would lead to charge separation and the loss of confinement due to the rising $\mathbf{E} \times \mathbf{B}$ drift. However for finite q the particles spend half of their times (in, say, the upper half of the torus) diverging from a given flux surface and half of their times (in the lower half) approaching the same flux surface again, thus having no net radial drift on time average.

The magnetic field strength decreases with major radius as $1/R$, which leads to yet another complication in the motion of the particles. Particles having too high magnetic moment compared to their kinetic energy cannot make a complete poloidal turn as they are reflected back from the higher field strength regions by the magnetic mirror force; these are the *trapped particles* which constitute a $\sim\sqrt{\epsilon}$ fraction of the particles, where we introduced the inverse aspect ratio $\epsilon = r/R$. These particles bounce back and forth in the outboard side of the tokamak with a poloidal projection of their guiding center trajectory having a banana shape; hence the often used name for the trapped particle orbits: *banana orbits*.

It is clear that for stationary fields the total energy of a particle $mv^2/2 + e_a\Phi$ has to be a constant of motion, where Φ is the electro-

static potential. In magnetized plasmas, the magnetic moment of a particle μ is an adiabatic invariant, which means that for slow (spatial and temporal) changes in the magnetic field strength the perpendicular velocity of the particles also changes keeping the quantity $\mu = mv_\perp^2/(2B)$ a constant. In perfect toroidally symmetric configurations there is an additional constant of motion, the canonical angular momentum $\Psi_* = -RA_\varphi - mRv_\varphi/e_a = \Psi - mRv_\varphi/e_a$, which follows from that the Lagrangian is independent of the toroidal angle φ (we introduced the toroidal components of the velocity and the magnetic vector potential, v_φ and A_φ respectively). This condition guarantees that the collisionless orbits are confined (i.e., restricted to a radially bounded domain) in tokamaks. In magnetized plasmas not only Ψ_* is conserved, but also the canonical angular momentum of the guiding centers $\bar{\Psi}_*$.

2.3 Distribution function and kinetic equations

The main objective of the kinetic theory of plasmas is to determine the phase space *distribution functions* of the different plasma particle species $f_a(t, \mathbf{r}, \mathbf{v})$, from which – taking their appropriate moments and averages – the desired macroscopic quantities, such as fluxes, flows, currents, can be calculated. The evolution of the distribution functions is determined from the Vlasov equation which is a local conservation equation for the distribution function:

$$\frac{df_a}{dt} \equiv \frac{\partial f_a}{\partial t} + \mathbf{v} \cdot \nabla f_a + \frac{e_a}{m_a} (\mathbf{E} + \mathbf{v} \times \mathbf{B}) \cdot \frac{\partial f_a}{\partial \mathbf{v}} = 0, \qquad (2.4)$$

where $e_a(\mathbf{E} + \mathbf{v} \times \mathbf{B})/m_a$ is the acceleration due to the Lorentz force. The electric and magnetic fields appearing in Eq. (2.4) can be separated to macroscopic fields, i.e. fields averaged over several Debye length, and microscopic fields that are strongly fluctuating on spatial scales comparable to or smaller than the Debye length due to the discreteness of the particles. The effect of the latter can be collected to a *collision operator* $C_a[f_a] = \partial f_a|_{coll}$ which describes the change in the distribution as a result of collisions. The resulting kinetic equation, called *Fokker-Planck equation*, is formally similar to Eq. (2.4) with two differences; the appearing $\mathbf{E}$ and $\mathbf{B}$ now represent the macroscopic fields, and the right hand side is equal to $C_a[f_a]$. Not only does the collision operator introduce coupling between the different species (noting that $C_a[f_a] = \sum_j C_{aj}[f_a, f_j]$, where C_{aj} describes collisions between species a

and j), but the distributions of all species appear implicitly in Eq. (2.4) as sources to the macroscopic electric and magnetic fields.

The Fokker-Planck equation together with the Maxwell's equations provide a complete and self-consistent description of plasmas, however this system of equations applied to realistic problems is intractably complex. Realizing that for the description of collisional or turbulent transport processes it is usually unnecessary to resolve time scales corresponding to the fast ion cyclotron motion, the problem can be significantly simplified. A gyro-phase averaging can be performed on the full kinetic equation – making use of the smallness of the gyro-radius compared to the equilibrium scales – to obtain the simpler drift kinetic or gyrokinetic equations for the gyro-center distribution. The drift kinetic equation used mainly in the theory of collisional transport considers toroidally symmetric fields and represents the particle as a drifting guiding center with a charge and magnetic dipole moment corresponding to the gyration of the particle. The gyrokinetic equation allows for sharp spatial variations in the perturbed fields and distributions on the scale of the ion or electron gyro radius, thus it is more suited for the description of turbulent transport.

Having calculated the distribution function of the different species the most important transport quantities, the flux surface average of the radial particle and energy fluxes (Γ_a and Q_a, respectively) can be calculated as

$$\langle \Gamma_a \cdot \nabla\Psi \rangle = \left\langle \int d^3v f_a \mathbf{v} \cdot \nabla\Psi \right\rangle, \tag{2.5}$$

and

$$\langle Q_a \cdot \nabla\Psi \rangle = \left\langle \int d^3v \frac{m_a v^2}{2} f_a \mathbf{v} \cdot \nabla\Psi \right\rangle, \tag{2.6}$$

where $\langle \cdot \rangle$ denotes the flux surface average.

Chapter 3

Neoclassical transport

In toroidally symmetric magnetic configurations, which we consider henceforth, such as in tokamaks, in the absence of collisions and fluctuations in local plasma parameters, the trajectories of plasma particles would remain within a radially bounded domain. This result, following from the conservation of the toroidal canonical momentum of the guiding centers, would mean no net radial transport. However, in reality, collisions can move particles from one unperturbed orbit to another, which, on the long term, leads to a diffusive transport of particles and heat across flux surfaces.

Even in a cylindrical magnetized plasma there is a radial transport due to collisions. The collisionless orbits are determined by the Larmor gyration of particles around the magnetic field lines and a free streaming of their guiding centers along the field lines. Collisions, by changing the particle velocity perpendicularly to the magnetic field, can relocate the particle from its gyro-orbit to another. The magnitude of the resulting transport can be estimated with a random-walk argument. The particle (electron or ion) diffusivity $D_e = D_i$ is proportional to $\nu_{ei}\rho_e^2 = \nu_{ie}\rho_i^2$, where ν_{ei} (ν_{ie}) is the electron-ion (ion-electron) collision frequency and ρ_e (ρ_i) is the electron (ion) Larmor radius.

Only unlike particle collisions lead to particle transport, because in like-particle collisions (i.e. electron-electron or ion-ion collisions) the average guiding center position does not change. In an unlike particle collision the electron step length ($\sim\rho_e$) is a square root of electron-to-ion mass ratio $\sqrt{m_e/m_i}$ smaller than the ion step length ($\sim\rho_i$), but this is balanced by that the electron-ion collision frequency is a factor m_e/m_i larger than the ion-electron collision frequency. Therefore the resulting

electron and ion fluxes are equal $\Gamma_e = \Gamma_i$. Consequently, the collisional particle transport does not lead to charge separation; this feature is called ambipolarity. The ambipolar property of the particle transport, which originates in the momentum conservation of the Coulomb collisions, persists in the presence of radial electric fields and even in toroidal geometry (in the lowest order in $\delta = \rho_i/L(\ll 1)$, where L represents the radial length scale).

Since energy can be transferred in like-particle collisions there is no condition for heat transport analogous to ambipolarity. In particular the collisional ion energy transport is dominated by ion-ion collisions and is typically a square root of ion-to-electron mass ratio larger than electron energy transport; in terms of ion and electron energy diffusivities $\chi_i \sim \nu_{ii}\rho_i^2$, while $\chi_e \sim \nu_{ee}\rho_e^2$.

3.1 Collisional transport across flux surfaces

To understand the origin of the collisional transport fluxes in toroidal geometry it is useful to introduce the fluid equations first. By taking the $\{1, m\mathbf{v}, mv^2/2\}$ velocity moments of the Fokker-Planck equation

$$\frac{df_a}{dt} \equiv \frac{\partial f_a}{\partial t} + \mathbf{v}\cdot\nabla f_a + \frac{e_a}{m_a}\left(\mathbf{E} + \mathbf{v}\times\mathbf{B}\right)\cdot\frac{\partial f_a}{\partial \mathbf{v}} = C_a[f_a], \tag{3.1}$$

we obtain the conservation equations for particles, momentum and energy [27]:

$$\frac{\partial n_a}{\partial t} + \nabla\cdot(n_a\mathbf{V}_a) = 0, \tag{3.2}$$

$$\frac{\partial m_a n_a \mathbf{V}_a}{\partial t} + \nabla_a\cdot\mathbf{\Pi}_a = ne(\mathbf{E} + \mathbf{V}\times\mathbf{B}) + \int d^3v\, C[f] m\mathbf{v}, \tag{3.3}$$

$$\frac{\partial}{\partial t}\left(\frac{3nT}{2} + \frac{mnV^2}{2}\right) + \nabla\cdot\mathbf{Q} = en\mathbf{E}\cdot\mathbf{V} + \int d^3v\, C[f]\frac{mv^2}{2}, \tag{3.4}$$

where we suppressed the species index, and introduced the fluid velocity $\mathbf{V} = \langle\mathbf{v}\rangle_f$, the temperature $T = \langle mv^2\rangle_f/3$, the momentum flux tensor $\mathbf{\Pi} = \langle mn\mathbf{v}\mathbf{v}\rangle_f$ and the energy flux $\mathbf{Q} = mn\langle v^2\mathbf{v}\rangle_f/2$, and the average over the distribution $n\langle\cdot\rangle_f = n_a^{-1}\int\cdot f d^3v$. We can denote the last term on the right hand side of Eq. (3.3) by $\mathbf{F}_a$ (representing the collisional friction force between different species).

It is easy to show using Eq. (2.3) that the flux surface average of the particle flux can be written as

$$\langle\Gamma_a\cdot\nabla\Psi\rangle = \langle R\hat{\varphi}\cdot(n_a\mathbf{V}_a\times\mathbf{B})\rangle, \tag{3.5}$$

with the toroidal unit vector $\hat{\varphi}$. Using this identity and taking the flux surface average of the toroidal projection of Eq. (3.3) then yields

$$\langle \Gamma_a \cdot \nabla \Psi \rangle = \frac{1}{e_a} \left\langle R\hat{\varphi} \cdot \frac{\partial m_a n_a \mathbf{V}_a}{\partial t} + R\hat{\varphi} \cdot \nabla \cdot \mathbf{\Pi}_a - n_a e_a R E_\varphi - R F_{a\varphi} \right\rangle, \quad (3.6)$$

where φ indices denote the toroidal component of a vector. Assuming that the plasma parameter profiles evolve due to collisional diffusion ($D \sim \nu\rho^2$) the time derivatives should be small $\partial_t \sim D/L^2 \sim \delta^2\nu$. From this estimate the first term in the right hand side of Eq. (3.6) is at least δ^2 smaller than the last term, even for flow velocities comparable to the thermal velocity. The second term would not be small if it contained contributions from the diagonal of the pressure tensor (i.e. the scalar pressure), but the pressure gradient does not appear due to axisymmetry ($\hat{\varphi} \cdot \nabla p = 0$). For similar reason ($\hat{\varphi} \cdot \nabla \Phi = 0$) in the third term (the so called Ware-pinch) only the induced electric field appears. The last term arising due to friction between the different species is responsible for the collisional transport.

The transport caused by the perpendicular friction is called the classical transport, while the so called *neoclassical* transport [28] which usually dominates in large aspect ratio tokamaks is due to the combined effect of the parallel induced electric field $E_{\parallel(\mathrm{ind})}$ and the parallel friction $F_\parallel$. The neoclassical particle flux can be written as

$$\langle \Gamma_a \cdot \nabla \Psi \rangle_{\mathrm{neo}} = -I \left\langle \frac{F_{a\parallel} + n_a e_a E_{\parallel(\mathrm{ind})}}{e_a B} \right\rangle. \quad (3.7)$$

3.2 Drift kinetic equation

The neoclassical fluxes can also be constructed kinetically; the particle and energy fluxes can be written in terms of the distribution function and the drift velocity formally as Eqs. (2.5) and (2.6) with the replacement $\mathbf{v} \to \mathbf{v}_d$. The distribution function appearing in the expression for the fluxes can be calculated from the *drift kinetic equation*. To derive this equation, we will follow the approach of Catto et al [29]. Again, we start with the Fokker-Planck equation (3.1), but rewrite it in a more convenient set of velocity space coordinates: the total energy per particle mass $\mathcal{E} = v^2/2 + e_a\Phi/m_a$ that is a constant of motion for time independent electrostatic potential Φ and in the absence of induced electric

fields (we do not consider the relativistic case, when the particle mass is not constant), the magnetic moment per particle mass $\mu = v_\perp^2/(2B)$ that is an adiabatic invariant, and the gyro-angle φ. In these coordinates the magnitude of the different velocity components are $v_\perp^2 = 2\mu B$ and $v_\parallel^2 = 2[(\mathcal{E} - e_a\Phi/m_a) - \mu B]$.

In an arbitrary set of phase space coordinates $\{z_i\}_{i=1}^6$ the kinetic equation can be written as

$$\partial_t f + \sum_{k=1}^{6} \dot{z}_k \partial f/(\partial z_k) = C[f], \tag{3.8}$$

where the time derivative is taken at fixed $\mathbf{z}$ and the partial derivative with respect to any z_k is taken keeping all the other phase space coordinates and the time fixed. The over-dot acting on any quantity Q denotes $\dot{Q} \equiv \partial_t Q + \mathbf{v}\cdot\nabla Q + (e_a/m_a)\,(\mathbf{E} + \mathbf{v}\times\mathbf{B})\cdot\partial_{\mathbf{v}} Q$. Accordingly,

$$\frac{\partial f_a}{\partial t} + \dot{\varphi}\frac{\partial f_a}{\partial \varphi} + \dot{\mathcal{E}}\frac{\partial f_a}{\partial \mathcal{E}} + \dot{\mu}\frac{\partial f_a}{\partial \mu} + \mathbf{v}\cdot\nabla f_a = C_a[f_a]. \tag{3.9}$$

It can easily be shown that, assuming $E_\parallel \ll E_\perp$, to lowest order in δ the total time derivatives of the velocity space coordinates are

$$\begin{aligned}
\dot{\mathcal{E}}_0 &= \frac{e_a}{m_a}\mathbf{v}_\perp\cdot(\mathbf{E} + \nabla\Phi) \\
\dot{\mu}_0 &= -\frac{\mu}{B}\mathbf{v}\cdot\nabla B - \frac{v_\parallel}{B}\mathbf{v}\cdot\nabla\mathbf{b}\cdot\mathbf{v} + \frac{e_a}{m_a B}\mathbf{v}_\perp\cdot\mathbf{E} \\
\dot{\varphi}_0 &= -\Omega_a.
\end{aligned} \tag{3.10}$$

Since the largest term in Eq. (3.9) is the one describing the Larmor rotation ($\propto \dot{\varphi}$), the lowest order kinetic equation is

$$-\Omega_a\frac{\partial f_0}{\partial \varphi} = 0, \tag{3.11}$$

where the distribution function is given as a series $f = f_0 + f_1 + \ldots$ $[f_{i+1}/f_i = \mathcal{O}(\delta)]$. Equation (3.11) implies that the lowest order distribution is gyro-phase independent. To next order we get

$$-\Omega_a\frac{\partial f_1}{\partial \varphi} + \dot{\varphi}_1\frac{\partial f_0}{\partial \varphi} + \dot{\mathcal{E}}_0\frac{\partial f_0}{\partial \mathcal{E}} + \dot{\mu}_0\frac{\partial f_0}{\partial \mu} + \mathbf{v}\cdot\nabla f_0 = C_0[f_0]. \tag{3.12}$$

The gyro-phase average of this equation provides a constraint on f_0

$$v_\parallel\mathbf{b}\cdot\nabla f_0 = C_0[f_0], \tag{3.13}$$

where we used that on gyro-phase average the terms containing φ-derivatives of single valued functions should vanish, and $\langle\dot{\mathcal{E}}_0\rangle_\varphi = 0 = \langle\dot{\mu}_0\rangle_\varphi$, furthermore the lowest order term in the gyro averaged velocity is the parallel streaming. Taking the transit average of Eq. (3.13) over a full bounce period for trapped particles and over a complete poloidal circuit for the passing particles annihilates the left hand side of the equation yielding

$$\oint d\tau C[f_0] = \oint \frac{d\theta}{v_\parallel \mathbf{b}\cdot\nabla\theta} C[f_0] = 0,$$

where τ denotes time. This constraint has the solution

$$f_0 = \eta_a \left(\frac{m_a}{2\pi T_a}\right)^{3/2} e^{-m_a\mathcal{E}/T_a} = n_a \left(\frac{m_a}{2\pi T_a}\right)^{3/2} e^{-m_a v^2/(2T_a)},$$

that is a Maxwellian distribution, with $\eta_a(\mathbf{r}) = n_a(\mathbf{r})\exp[e_a\Phi(\mathbf{r})/T(\mathbf{r})]$. But the collision operator acting on a Maxwellian should vanish (since the system reached local thermodynamic equilibrium), thus Eq. (3.13) reduces to

$$v_\parallel \mathbf{b}\cdot\nabla f_0 = 0. \tag{3.14}$$

Since $v_\parallel$ is arbitrary, this new constraint implies that f_0 should be constant along the field lines, which – together with the requirement of f_0 being continuous – means that the lowest order distribution (and also η_a) should be a flux function $f_0 = f_0(\Psi, \mathcal{E})$.

To calculate the first order distribution f_1 it is more convenient to employ the canonical angular momentum $\Psi_* = \Psi - m_a R\hat{\zeta}\cdot\mathbf{v}/e_a$ (where $\hat{\zeta}$ is the unit vector pointing in the toroidal direction) that is a constant of the motion ($\dot{\Psi}_* = 0$). Considering Ψ_* as a phase space variable we can define the distribution

$$f_*(\Psi_*, \mathcal{E}) = \eta_*(\Psi_*) \left(\frac{m_a}{2\pi T_a(\Psi_*)}\right)^{3/2} e^{-m_a\mathcal{E}/T_a(\Psi_*)}$$

which has a very simple total time derivative

$$\dot{f}_* = \dot{\Psi}_* \frac{\partial f_*}{\partial \Psi_*} + \dot{\mathcal{E}}\frac{\partial f_*}{\partial \mathcal{E}} + \frac{\partial f_*}{\partial t} = \dot{\mathcal{E}}\frac{\partial f_*}{\partial \mathcal{E}} + \frac{\partial f_*}{\partial t}.$$

We can write the distribution function as $f = f_* + h$ which, inserted in the full kinetic equation (3.9), gives

$$\dot{h} + \dot{\mathcal{E}}\frac{\partial f_*}{\partial \mathcal{E}} + \frac{\partial f_*}{\partial t} = C[f_* + h]. \tag{3.15}$$

Writing the unknown part of the distribution $h = h_1 + h_2 + \ldots$, using that $\dot{\mathcal{E}} = e_a[\partial_t \Phi - \mathbf{v} \cdot (\partial_t \mathbf{A})]/m_e$ is small according to the transport ordering, to lowest order we find

$$-\Omega_a \frac{\partial h_1}{\partial \varphi} = C_0[f_0] = C_0[f_M] \equiv 0,$$

thus h_1 is independent of the gyro-angle. Using this fact, the next order equation can be written as

$$-\Omega_a \frac{\partial h_2}{\partial \varphi} + \mathbf{v} \cdot \nabla h_1 + \dot{\mu} \frac{\partial h_1}{\partial \mu} + \frac{e_a}{m_a} \mathbf{v} \cdot (\mathbf{E} + \nabla \Phi) \frac{\partial f_0}{\partial \mathcal{E}} = C[f_* + h_1]. \quad (3.16)$$

Since the collision operator acting on a Maxwellian is zero, we can make the replacement $C[f_* + h_1] \to C[f_* - f_0 + h_1]$.

Gyro-averaging Eq. (3.16) leads to the drift kinetic equation

$$v_\parallel \mathbf{b} \cdot \nabla h_1 - \frac{e_a}{T_a} f_0 v_\parallel \mathbf{b} \cdot (\mathbf{E} + \nabla \Phi) = C_l \left[h_1 - \frac{I v_\parallel}{\Omega_a} \frac{\partial f_0}{\partial \Psi} \right], \quad (3.17)$$

where we used that the gyro-average of $\dot{\mu}$ vanishes, and approximated f_* by its Taylor expansion about Ψ to the first order

$$f_* = f_M(\mathcal{E}, \Psi) + (\Psi_* - \Psi) \frac{f_M}{\partial \Psi}\bigg|_{\mathcal{E}} + \cdots \approx f_0 - \frac{m_a}{e_a} R\hat{\zeta} \cdot \mathbf{v} \frac{\partial f_0}{\partial \Psi}\bigg|_{\mathcal{E}}. \quad (3.18)$$

In Eq. (3.17) we approximated the Coulomb collision operator C with the linearized collision operator C_l and used the rotational symmetry of C_l to write $\langle C_l[f_* - f_0 + h_1] \rangle = C_l[\langle f_* - f_0 \rangle + h_1]$. For ions the second term in the left hand side of Eq. (3.17) arising due to the induced electric field is negligibly small, furthermore usually only the ion-ion collisions need to be taken into account. The electron drift kinetic equation is more complicated as the electrons are collisionally coupled to the ions, and the effect of the induced electric field is not negligible. It can simplify the latter problem if the solution f_S of the *Spitzer problem*

$$C_l[f_S] = \frac{e}{T_e} f_{0e} v_\parallel \mathbf{b} \cdot (\mathbf{E} + \nabla \Phi)$$

is known.

The drift kinetic equation is sometimes written in an alternative form. The gyro-average of the first order correction to the lowest order Maxwellian can be written as

$$\bar{f}_1 = h_1 - \frac{I v_\parallel}{\Omega_a} \frac{\partial f_0}{\partial \Psi}\bigg|_{\mathcal{E}}.$$

Realizing that the radial component of the guiding center drift velocity [Eq. (2.1)] can be conveniently expressed as

$$\mathbf{v}_d \cdot \nabla\Psi = I v_\parallel \mathbf{b} \cdot \nabla|_{\mathcal{E},\mu} \left(\frac{v_\parallel}{\Omega_a} \right), \tag{3.19}$$

the drift kinetic equation for $\bar{f}_1$ can be easily derived

$$v_\parallel \mathbf{b} \cdot \nabla|_{\mathcal{E},\mu} \bar{f}_1 - C_l \bar{f}_1 = - \mathbf{v}_d \cdot \nabla\Psi \frac{\partial f_0}{\partial \Psi}\bigg|_{\mathcal{E}} + \frac{e_a}{T_a} f_0 v_\parallel \mathbf{b} \cdot (\mathbf{E} + \nabla\Phi). \tag{3.20}$$

3.3 Collisionality regimes

Depending on the relative magnitudes of the effective collision frequency ν_{eff} – that is, the typical frequency of the collisional de-trapping of trapped particles – and the typical frequencies for the circulating and trapped particles to complete a full orbit (a full poloidal circuit or a banana orbit respectively), we can identify three collisionality regimes. In the low collisionality limit, the so called *banana* regime that is typical in the high temperature core in the tokamaks, both trapped and circulating particles can complete their orbits before they become de-trapped/trapped by collisions. In the high collisionality limit, that is called the *Pfirsch-Schlüter* (PS) regime, both circulating and trapped particle orbits are frequently interrupted by collisions. For large aspect ratio ($\epsilon \ll 1$) there is a third, intermediate collisionality regime, the *plateau* regime, where the circulating particles are weakly collisional, like in the banana regime, but the trapped and barely passing particle orbits are frequently interrupted by collisions (due to the lower parallel velocity of these particles).

Mathematically, in the PS regime the typical mean free path v_T/ν is much smaller than the connection length qR, thus $\nu qR/v_T \gg 1$, while in the banana regime the effective collision frequency (the frequency of the collisional de-trapping of trapped particles $\nu_{\text{eff}} \sim \nu/\epsilon$) is much smaller than the bounce frequency $\omega_b \sim \sqrt{\epsilon} v_T/(qR)$, accordingly $\nu qR/v_T \ll \epsilon^{3/2}$. Finally, the plateau regime that occupies the range between these two is characterized by $\epsilon^{3/2} \ll \nu qR/v_T \ll 1$.

In the banana regime the main part of the radial collisional transport is caused by the trapped particles. Due to the magnetic drifts these particles have radially extended guiding center orbits. Using the conservation of the canonical angular momentum of the guiding centers $\bar{\Psi}_*$ the radial width of the banana orbits can be easily estimated as $\Delta_b \sim \sqrt{\epsilon}\rho_p$,

where $\rho_p = \rho B_t/B_p$ ($\gg \rho$) denotes the poloidal Larmor radius. Collisions, by interrupting and de-trapping particles at different points of their banana orbits can therefore cause a radial displacement of particles with a step length comparable to Δ_b, and in the long term they lead to a diffusive transport.

The diffusivity in the banana regime can be estimated from a random walk picture as $D_b \sim \sqrt{\epsilon}\nu_{\text{eff}}\Delta_b^2 \sim \nu\rho^2 q^2/\epsilon^{3/2}$, where the $\sqrt{\epsilon}$ factor comes from the trapped fraction. This diffusivity significantly exceeds the classical diffusivity $D_{cl} \sim \nu\rho^2$ discussed in the beginning of Chapter 3, as q is typically higher than unity (except really close to the magnetic axis) and ϵ is smaller than unity. To demonstrate that the contribution of the circulating particles is lower than that of the banana particles we note that a typical circulating particle gets trapped on the time scale of the collision frequency ν ($\ll \nu_{\text{eff}}$) and the radial extent of its orbit is smaller by a factor of $\sqrt{\epsilon}$ than a typical banana width, which leads to a diffusion coefficient $\sim q^2\rho^2\nu \ll D_b$.

In the PS regime the parallel motion of the particles is frequently interrupted by collisions and as they change directions they drift upwards or downwards with the magnetic drift frequency. We can use a random walk model to give an estimate for the diffusivity. The parallel step length is the mean free path $\lambda \sim v_T/\nu$ which gives a parallel diffusion coefficient $D_\parallel \sim \lambda^2\nu \sim v_T^2/\nu$. The time to go around the torus poloidally in a random walk fashion is therefore $\Delta t \sim (qR)^2/D_\parallel$. The radial step length is then $\Delta r \sim v_d\Delta t \sim \rho v_T\Delta t/R$, from which the radial PS diffusion coefficient can be calculated as $D_{PS} \sim (\Delta r)^2/\Delta t \sim \nu\rho^2q^2$. Since this collisionality regime is typical in the plasma edge, where the safety factor q is larger than unity, the PS transport also exceeds the classical transport.

The diffusion coefficients in both of the above collisionality regimes exhibit a linear dependence on collision frequency. Interestingly for intermediate collisionalities, where the passing particles are collisionless and the trapped ones are collisional (i.e. the plateau regime), the diffusion coefficients become independent of collision frequency, although the transport is caused by collisions. This is rather convenient since the details of the collision process (and the form of the collision operator used) become unimportant. The transport in the plateau regime is caused by a resonance between the transit- and collision frequencies of slowly circulating particles [mathematically: slowly as $(v_\parallel/v)^3 \sim \nu qR/v \ll 1$, but circulating $\sqrt{\epsilon} \ll v_\parallel/v (\doteq \xi)$]. To give a simple random walk es-

timate in this region the usual $(\Delta r)^2/\Delta t$ should be multiplied by the fraction of the resonant particles $\mathcal{F} \sim \xi \sim (\nu q R/v)^{1/3}$. The step time is the inverse of the effective collision frequency $\nu_{\text{eff}} = \nu/\xi^2$ and the step size is $\Delta r \sim v_d/\nu_{\text{eff}}$, which leads to diffusivities with the magnitude $D_p \sim q\rho^2 v_T/R$. Not surprisingly, this estimate is obtained if we replace $\nu q R/v_T$ by $\epsilon^{3/2}$ in the banana diffusivity estimate or by 1 in the PS estimate. The collisionality dependence of the neoclassical diffusivity in the banana, plateau and P-S collisionality regimes is illustrated in Fig. 3.1.

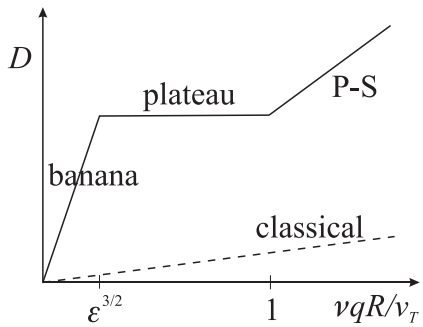

Figure 3.1: Classical (dashed) and neoclassical (solid) diffusivities as functions of the collisionality in large aspect ratio ($\epsilon \ll 1$). For increasing ϵ the neoclassical diffusivity curve becomes more and more smooth and the plateau region shrinks until it completely disappears for $\epsilon \sim \mathcal{O}(1)$.

To demonstrate how transport arises in the plateau regime we solve the ion drift kinetic equation, which, after introducing the distribution

$$H_i = h_{1i} - \frac{I v_\parallel f_{0i}}{\Omega_i T_i}\left(\frac{m_i v^2}{2T_i} - \frac{5}{2}\right)\frac{\partial \ln T_i}{\partial \Psi},$$

and considering a large aspect ratio circular cross section plasma, can be written in the form of

$$\xi \frac{\partial H_i}{\partial \theta} + \frac{\nu_{\text{eff}} q R}{v} H_i = Q_i \sin\theta, \tag{3.21}$$

where Q_i is a source term proportional to the ion temperature gradient, and the collision is modeled with a simple Krook operator $C[H_i] \to -\nu_{\text{eff}} H_i$. The radial fluxes are calculated as the flux surface average of certain velocity moments of $f\mathbf{v}_d \cdot \hat{r}$, and we know that $\mathbf{v}_d \cdot \hat{r} \propto \sin\theta$, so only that part of the solution H_i of Eq. (3.21) which is odd in theta

needs to be kept. It is easy to show that

$$H_{i(\mathrm{odd})} = Q_i \frac{\Delta}{\xi^2 + \Delta^2} \sin\theta,$$

where $\Delta = \nu_{\mathrm{eff}} qR/v \ll 1$. In the $\Delta \to 0$ limit the function $\Delta/(\xi^2 + \Delta^2)$ approaches a Dirac delta function times a constant. Physically it means that mainly those particles contribute to the transport for which $\xi = v_\parallel/v$ is small enough that it becomes comparable to Δ, that is, the ones having similar effective collision frequencies and transit frequencies. We note that using more sophisticated collision operators would lead to the same result [27].

3.4 Bootstrap current

In a cylindrical straight field line geometry parallel current arises only due to parallel electric field and is determined by the conductivity. This contribution to the total current in toroidal geometry is called the Spitzer current (or ohmic current). However in the toroidal case there are further components of the parallel current. Since the surface area of a flux surface in the outboard side is higher than in the inboard side, and the kinetic pressure is constant on a flux surface, a force pointing towards the outboard side is acting on the plasma column. There are perpendicular currents flowing within the flux surfaces to counteract this effect by their $\mathbf{J} \times \mathbf{B}$ force. To make the total current divergence free a parallel return current, the Pfirsch-Schlüter current, arises. This current has opposite directions in the inboard and outboard sides and vanishes on flux surface average. Apart from the ohmic and PS currents there is a further component of the total parallel current that does not vanish on flux surface average, the so called bootstrap current generated by density and temperature gradients.

To understand the physical mechanism behind the bootstrap current, first we introduce the concept of diamagnetic flow. A particle orbit deviates from the a given magnetic surface to a certain extent partly because of the finite Larmor radius of the particle and partly due to the drifts of the guiding center. The former effect is present even in cylindrical geometry, and having radial gradients in the density and temperature of the species causes a fluid flow perpendicularly to the field lines [in the direction of $\mathrm{sign}(e_a)\mathbf{b} \times \nabla\{n, T\}$, the so called *diamagnetic direction*]. In a certain spatial point there are particles passing with their

guiding centers being in the higher or the lower density (temperature) region; these two groups of particles have opposite velocity components in the diamagnetic direction. Since in the higher density (temperature) region there are more particles (having higher velocity), there will be more particles moving in the diamagnetic direction than the opposite direction, hence causing a net flow, that turns out to be proportional to the pressure gradient. This is a purely fluid flow, since the particle guiding centers (the average position of particles with regard to a field line) are staying still.

In toroidal geometry, the magnetic drift of particles causes even larger deviations from a reference flux surface (for trapped particles comparable to the banana width). The particles are mainly moving parallel to the field lines but due to the drifts they pass higher and lower pressure regions, which, by a process analogous to the one causing the usual diamagnetic flow, generates a parallel flow, again, proportional to the gradients in plasma profiles (see the illustration in Fig. 3.2).

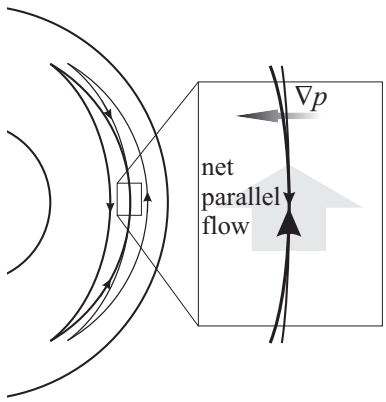

Figure 3.2: Parallel diamagnetic flow of trapped particle guiding centers (top view).

It can be shown that the diamagnetic flow of the passing electrons is higher than that of the trapped ones by a factor of $\epsilon^{-1/2}$, even though the banana width is larger than the deviation of circulating orbits from flux surfaces. Electron-electron collisions conserve momentum, therefore the momentum loss of trapped electrons in collisions with the circulating ones and the momentum loss of circulating particles in collisions with the trapped ones should balance. If the parallel flows would simply

consist of the diamagnetic flows caused by the guiding center motion, the parallel momentum balance could not be achieved. Accordingly there should be an additional parallel flow of circulating particles, which is – interestingly – even higher than the diamagnetic flow of these particles. This flow produces the bootstrap current.

For radially monotonically decreasing density and temperature profiles (which is almost always the case) the bootstrap current has the same direction as the ohmic current, thus reducing the need of the ohmic current drive which limits the length of the plasma discharges. Therefore, it is considered to be advantageous for reactor relevant operation of tokamaks. However, it can be shown that a tokamak cannot operate on purely bootstrap current because the decreasing gradients towards the magnetic axis would lead to magnetohydrodynamically unstable magnetic configurations. The bootstrap current also plays an important role as a destabilizing factor for certain MHD instabilities.

3.5 Neoclassical transport in H-mode pedestals

The deviation of guiding centers from flux surfaces (the *orbit width*) scales as the poloidal Larmor radius ρ_p, although formally smaller than that by a factor of $\sqrt{\epsilon}$ for trapped and ϵ for circulating particles. However in realistic magnetic geometries at the edge $\sqrt{\epsilon}$ can be $\mathcal{O}(1)$, and the banana width becomes comparable to ρ_p. There is experimental evidence showing that the density length scale in an H-mode pedestal can also be as small as the poloidal Larmor radius of ions, which causes two problems. Most of the drift kinetic and gyrokinetic treatments assume that the orbit width of the particles is much smaller than the scale lengths of the background parameters, which might be violated in the pedestal. Another problem is that, assuming sub-sonic toroidal rotation of ions, the lowest order ion pressure balance equation requires the existence of a strong radial electric field

$$\frac{d\Phi}{dr} \approx -\frac{T_i}{e_i}\frac{d\ln n_i}{dr},$$

that significantly modifies the ion orbits. In particular, electrostatic trapping of particles becomes important and the trapped region can be shifted towards the tail of the distribution for sufficiently large radial electric fields, as it is illustrated in Fig. 3.3.

In neoclassical theory the fact, that the radial drift term in the kinetic equation [first term in the right hand side of Eq. (3.20)] can be

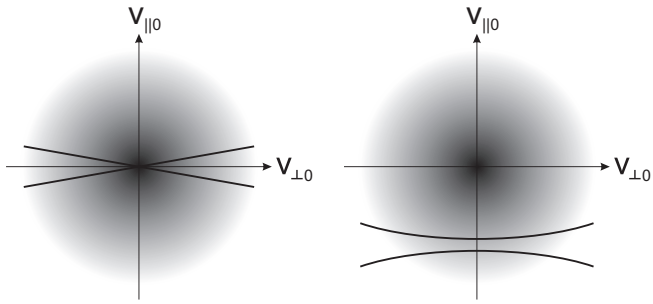

Figure 3.3: Location of the trapped region in velocity space in the weak radial electric field limit (left) and for finite electric field (right). The lowest order Maxwellian distribution is indicated with a gray-scale density plot.

expressed in terms of the parallel motion as in Eq. (3.19), is often used to mathematically simplify the problem since this form has similar structure to the parallel streaming term [the first term in the left hand side of Eq. (3.20)]. This can only be done though, when the poloidal motion of particles is dominated by the parallel streaming ($\mathbf{v} \cdot \nabla\theta = v_{\|}\mathbf{b} \cdot \nabla\theta$ in lowest order), which is usually the case. However, in the pedestal the $\mathbf{E} \times \mathbf{B}$ drift in the strong radial electrostatic field can have a comparable contribution to the poloidal motion. For this reason, $\mathbf{v}_{\mathbf{E}\times\mathbf{B}}$ needs to be kept in the same order in the formalism as $\mathbf{v}_{\|}$, but since $\mathbf{v}_{\mathbf{E}\times\mathbf{B}} \cdot \nabla\theta$ cannot be expressed in terms of the parallel velocity the above simplifying trick cannot be applied. To make progress, another approach can be used in which the canonical angular momentum (or its gyro-average) replaces the poloidal flux as one of the independent variables, which is convenient because $\dot{\Psi}_*(\partial\ \cdot)/(\partial\Psi_*) = 0$. This method which makes clear the distinction between transit averages and flux surface averages was developed by Kagan and Catto [30]. As a complement to their banana regime calculation, we calculate the corrections to the neoclassical plateau regime transport retaining finite $\mathbf{E} \times \mathbf{B}$ departures from flux surfaces in paper C. An overview of these results completed by a zonal flow residual calculation can be found in Ref. [G].

Chapter 4

Turbulent transport and microinstabilities

It was recognized from early fusion experiments that the heat transport across the flux surfaces is so high that it cannot be explained purely by collisional processes, even taking the neoclassical corrections into account. As will become clear in the sequel, turbulent flows of the plasma, referred traditionally as *anomalous* transport, account for the major part of the particle and heat fluxes. The turbulence is driven by different drift-type microinstabilities that are destabilized by inhomogeneities in the plasma parameters.

A rough estimate of the turbulent transport can be obtained using a simple random walk estimate, assuming that the step length Δ is comparable to the ion thermal Larmor radius $\rho_T = v_T/\Omega_c$ and the step time τ scales as the inverse of a typical (magnetic or diamagnetic) drift frequency $\sim k_\theta \rho_T v_T/a \sim v_T/a$, where we used that the perpendicular wave length $\sim 1/k_\theta$ is also comparable to the Larmor radius and the scale lengths of plasma parameters scale as the minor radius of the device a. This leads to the gyro-reduced Bohm (or simply "gyro-Bohm" [32]) scaling

$$D \sim \Delta^2/\tau \sim \rho_T^2 \frac{v_T}{a} \sim \frac{\rho_T}{a}\frac{T}{eB}. \tag{4.1}$$

The level of transport is determined by the saturation amplitude of the perturbed quantities, and therefore the assumption of different saturation mechanisms leads to different diffusivities. One widely used approach is the mixing-length estimate [33], which balances the drift wave drive due to gradients ($\sim \omega_{*\alpha}$) against the $\mathbf{E} \times \mathbf{B}$ nonlinearity

leading to a diffusivity $D \sim \gamma/k_\perp^2$, where γ is the linear growth rate of the most unstable mode. This is equivalent to a "wave breaking" picture, where the fluctuation amplitude saturates when the gradients of the perturbed quantities grow to the level of the equilibrium gradients

$$\nabla\hat{n} \sim \nabla n \Rightarrow k_\perp \hat{n} \sim n/L_n. \tag{4.2}$$

Assuming a Boltzmann relation between the density and potential perturbations, ($\hat{n}$ and $\hat{\phi}$ respectively), this implies $e\hat{\phi}/T \sim (k_\perp L_n)^{-1}$.

4.1 Gyrokinetic description

For investigating microinstabilities and for quantitative calculation of the turbulent fluxes one has to compute the distribution function of the different species, which can be done within the framework of gyrokinetic description of plasmas. This gyro-averaged kinetic description allows for short perpendicular wave lengths $k_\perp$ on the order of the (ion or electron) Larmor radius and frequencies ω much lower than the ion cyclotron frequency Ω_c. In terms of the small parameter $\delta = \rho/L \sim \rho/a$ the ordering of the gyrokinetic theory can be written as

$$\frac{\hat{f}_a}{f_a} \sim \frac{e_a\hat{\phi}}{T_a} \sim \frac{e_a v_{Ta}|\hat{\mathbf{A}}|}{T_a} \sim \frac{k_\parallel}{k_\perp} \sim \frac{\omega}{\Omega_{ca}} \sim \delta, \tag{4.3}$$

where hat denotes the perturbed quantities. This ordering is often completed by assuming slow variation of the ensemble-averaged quantities $\partial/\partial t \sim \delta^2$, the so called transport ordering.

In the recursive method of deriving the gyrokinetic equation [34] the distribution function is separated to perturbed $\hat{f}_a$ and equilibrium parts f_a and these together with the perturbed and equilibrium $\mathbf{B}$ and $\mathbf{E}$ fields are expanded in δ. The gyrokinetic equation is derived from the Fokker-Planck equation

$$\left[\frac{\partial}{\partial t} + \mathbf{v}\cdot\nabla + \frac{e_a}{m_a}\left((\mathbf{E}+\hat{\mathbf{E}}) + \mathbf{v}\times(\mathbf{B}+\hat{\mathbf{B}})\right)\cdot\frac{\partial}{\partial \mathbf{v}}\right](f_a + \hat{f}_a) = C_a[f_a + \hat{f}_a]. \tag{4.4}$$

From the ensemble average of Eq. (4.4) different orders of the drift kinetic equation can be derived, which, in particular, can be used to determine the lowest order equilibrium distribution that is considered to

be known in the gyrokinetic equation (and usually is a Maxwellian in a rotating frame of reference).

To obtain an equation for the perturbed distribution $\hat{f}_a$, we subtract the ensemble average of Eq. (4.4) from Eq. (4.4), yielding

$$\left[\frac{\partial}{\partial t} + \mathbf{v}\cdot\nabla + \frac{e_a}{m_a}\left(\mathbf{E}+\mathbf{v}\times\mathbf{B}\right)\cdot\frac{\partial}{\partial \mathbf{v}}\right]\hat{f}_a$$
$$= -\frac{e_a}{m_a}\left(\hat{\mathbf{E}}+\mathbf{v}\times\hat{\mathbf{B}}\right)\cdot\frac{\partial(f_a+\hat{f}_a)}{\partial\mathbf{v}} + C_a - \langle C_a\rangle_{\mathrm{ens}} - \mathcal{D}_a, \qquad (4.5)$$

where we introduced the fluctuation-particle interaction operator $\mathcal{D}_a = -(e_a/m_a)\langle(\hat{\mathbf{E}}+\mathbf{v}\times\hat{\mathbf{B}})\cdot\partial_{\mathbf{v}}\hat{f}_a\rangle_{\mathrm{ens}}$.

The gyro-average of Eq. (4.5) to first order provides a constraint for $\hat{f}_{a1}$ which should then have the form

$$\hat{f}_{a1}(\mathbf{x}) = -\frac{e_a\hat{\Phi}(\mathbf{x})}{T_a} + H_a(\mathbf{X}),$$

where the first term in the right hand side is called the adiabatic (or Boltzmann) part of the perturbed distribution and the second term is the non adiabatic part. The gyro-average of the next order equation leads to the gyrokinetic equation, which, in axisymmetric toroidal configuration, if the 0^{th} order toroidal rotation can be neglected, can be written as [34, 35]

$$\frac{\partial h_a}{\partial t} + (v_\parallel\mathbf{b}+\mathbf{v}_d)\cdot\nabla H_a + \hat{\mathbf{v}}_d\cdot\nabla h_a - C_a[H_a] = -\hat{\mathbf{v}}_d\cdot\nabla f_{a0}, \qquad (4.6)$$

where $\mathbf{v}_d$ is given in Eq. (2.1), and we introduced the perturbed drift velocity $\hat{\mathbf{v}}_d = \mathbf{b}\times\nabla\hat{U}/B$ and $h_a(\mathbf{X}) = H_a(\mathbf{X}) - e_a f_{a0}\hat{U}(\mathbf{X})/T_a$, with the following gyro-averaged $\langle\cdot\rangle_\varphi$ quantity

$$\hat{U}(\mathbf{X}) = \left\langle\hat{\Phi}(\mathbf{X}+\boldsymbol{\rho}) - \mathbf{v}\cdot\hat{\mathbf{A}}(\mathbf{X}+\boldsymbol{\rho})\right\rangle_\varphi. \qquad (4.7)$$

To allow for sharp variations perpendicularly to the field lines, the perturbed fields $\hat{Y}$ are expressed through the eikonal (or WKB) approximation

$$\hat{Y}(\mathbf{x}) = Y_*(\mathbf{X})e^{i\mathbf{k}_\perp\cdot\mathbf{x}}, \qquad (4.8)$$

where Y_* and $\mathbf{k}_\perp$ are spatially slowly varying functions. The gyro-average is

$$\langle\hat{Y}\rangle_\varphi(\mathbf{X}) = e^{i\mathbf{k}_\perp\cdot\mathbf{X}}Y_*\langle e^{i\mathbf{k}_\perp\cdot\boldsymbol{\rho}}\rangle_\varphi. \qquad (4.9)$$

The average can easily be evaluated in terms of the Bessel function of the first kind J_n, using that

$$J_n(z) = \frac{1}{2\pi} \oint d\gamma e^{-in\gamma + iz\sin\gamma}. \tag{4.10}$$

Thus we have

$$\begin{aligned} \langle e^{i\mathbf{k}_\perp \cdot \boldsymbol{\rho}} \rangle_\varphi &= J_0(k_\perp \rho), \\ \langle \mathbf{v}_\perp e^{i\mathbf{k}_\perp \cdot \boldsymbol{\rho}} \rangle_\varphi &= i v_\perp J_1(k_\perp \rho)(\mathbf{k}_\perp \times \mathbf{b})/k_\perp, \\ \langle \boldsymbol{\rho} e^{i\mathbf{k}_\perp \cdot \boldsymbol{\rho}} \rangle_\varphi &= i\rho J_1(k_\perp \rho)\mathbf{k}_\perp / k_\perp. \end{aligned} \tag{4.11}$$

Using these we find that

$$\begin{aligned} \hat{U}(\mathbf{X}) = J_0(k_\perp \rho_a) \left[\hat{\Phi}(\mathbf{X}) - v_\parallel \hat{A}_\parallel(\mathbf{X}) \right] \\ + \frac{1}{2} \left[J_0(k_\perp \rho_a) + J_2(k_\perp \rho_a) \right] \frac{v_\perp^2}{\Omega_{ca}} \hat{B}_\parallel(\mathbf{X}). \end{aligned} \tag{4.12}$$

In linear gyrokinetic calculations the nonlinearity in Eq. (4.6) represented by the $\hat{\mathbf{v}}_d \cdot \nabla h_a$ term is neglected. But even in the linear case the equation is a partial differential equation for which analytical solution can only be found in the simplest geometry and using further approximations. Usually the linear gyrokinetic equation is solved numerically either by looking for the asymptotic behavior of the time dependent coupled gyrokinetic-Maxwell system (this is the "initial value solver" approach), or by constructing a linear matrix equation from the discretized, Laplace-transformed problem and solving for its eigenmodes (this is the "eigenvalue solver" approach [35]). The advantage of the latter method is that it can find sub-dominant modes, while the initial value solver methods converge to the most unstable eigenmode.

4.2 Ballooning formalism

The turbulent fluctuations in plasmas are typically highly elongated along magnetic field lines (i.e. their parallel wave length $1/k_\parallel$ is comparable to the connection length qR), but they have a short perpendicular scale ($k_\perp \rho \sim 1$). The seemingly simplest way to represent such an elementary perturbation would be to write it as a flute-like mode: $\propto e^{i(m\chi - n\varphi)}$, χ and φ are the poloidal and toroidal coordinates respectively, and $m = nq$ with the integers m and n. However, this form turns

out to be useful only on a rational surface (i.e. a surface with rational q) and it is incompatible with the periodicity conditions in χ and φ as soon as q is irrational, that is, at any finite distance from the rational surface for finite magnetic shear.

The linear mode structure of microinstabilities is not localized around rational surfaces but rather it is radially extended over several rational surfaces (which are, in this case, close to each other due to the high toroidal mode number). Thus, instead of employing a flute-like expansion of the modes, it is more convenient to consider the problem in the ballooning representation which is appropriate for the description of mode structures characterized by short perpendicular and long parallel wavelengths when the magnetic shear is finite [36]. After separating the time dependence $e^{-i\omega t}$, using an eikonal representation, the n^{th} toroidal harmonic of the perturbed field $\hat{Y}$ can be expressed as $\hat{Y}_n(r,\chi,\varphi) = \hat{y}_n(r,\chi)e^{-in[\varphi - q(r)\chi]}$, which can further be written as

$$\hat{Y}_n(r,\chi,\varphi) = \sum_{\theta_0} \sum_{j=-\infty}^{\infty} \hat{Y}_{B,n}(\chi + 2\pi j, \theta_0) e^{-in[\varphi - q(r)(\chi + 2\pi j + \theta_0)]}, \quad (4.13)$$

where the ballooning function $\hat{Y}_{B,n}$ depending on the extended poloidal angle $\theta = \chi + 2\pi j \in \mathbb{R}$ has been introduced together with the ballooning angle θ_0, which acts as linear eigenmode label [37]. Physically θ_0 is the poloidal angle where the wave fronts are perpendicular to the flux surfaces. The originally two-dimensional problem for $\hat{y}_n(r,\chi)$ – with a periodicity condition in χ – now reduces to a series of one dimensional calculations for $\hat{Y}_{B,n}(\theta,\theta_0)$ with the much simpler condition $\hat{Y}_{B,n}(|\theta| \to \infty, \theta_0) \to 0$. In the limiting case of $\rho_* \to 0$, keeping N terms of the θ_0 series, so that $\theta_0 = \{2\pi l/N \mod 2\pi\}_{l=1}^{N}$, gives radially $N\Delta$ periodic eigenmode solutions, where $\Delta = (nq')^{-1}$ is the distance between the adjacent rational surfaces. The use of this expansion becomes apparent if we note that the most unstable mode can usually be calculated by considering only the $\theta_0 = 0$ term.

We would like to emphasize that the elementary modes in ballooning representation are radially periodic. Strictly speaking this would represent the reality only if the different geometry and plasma parameters were constant over the considered radial domain. However, to simplify the mathematical problem we can approximate these parameters (and their derivatives) with their value at a certain radial point within the considered radial domain (we might call this procedure the "flattening of the profiles"). This can be justified when the considered radial domain

is small compared to the size of the device (i.e. in the $\rho_* \to 0$ limit). Radial periodicity and flattening of the profiles are often imposed even in nonlinear simulations to increase computational efficiency, as in this case the differential operators appearing in the gyrokinetic-Maxwell system have no explicit dependence on radius and the binormal coordinate, thus the perturbed quantities can be Taylor-expanded in the perpendicular domain.

For a low-β, circular cross section, axisymmetric, large aspect ratio equilibrium the linearized gyrokinetic equation for the nonadiabatic part of the distribution g_a reads in the ballooning representation as [39]

$$\frac{v_\parallel}{qR}\partial_\theta g_a - i\left(\omega - \omega_{Da}\right) g_a - C[g_a] = -i\frac{e_a f_{a0}}{T_a}\left(\omega - \omega_{*a}^T\right)\phi J_0(z_a), \quad (4.14)$$

where $g = \hat{g}_{B,n}$ and $\phi = \hat{\Phi}_{B,n}$ in the notation of Eq. (4.13). Here, only purely electrostatic perturbations are considered $\{\hat{A}_\parallel, \hat{B}_\parallel\} = 0$, and $\theta_0 = 0$ is chosen. The time derivative is expressed in terms of wave frequency $\partial_t \to -i\omega$. Conventionally $\omega_{*a}^T = \omega_{*a}\left[1 + \left(x_a^2 - \frac{3}{2}\right) L_{na}/L_{Ta}\right]$, where ω_{*a} is the diamagnetic frequency, x_a is the velocity normalized to the thermal speed, $L_{na} = -\left[\partial_r(\ln n_a)\right]^{-1}$ and $L_{Ta} = -\left[\partial_r(\ln T_a)\right]^{-1}$ are the density and temperature scale lengths, $\omega_{Da} = k_\theta(v_\perp^2/2 + v_\parallel^2)(\cos\theta + s\theta\sin\theta)/(\Omega_a R)$ is the magnetic drift frequency (without the finite beta correction). The argument of the Bessel function being responsible for the finite Larmor radius effects is $z_a = k_\theta v_{\perp a}\sqrt{1 + s^2\theta^2}/\Omega_a$. The equilibrium distribution f_{a0} is taken to be Maxwellian.

4.3 Particle and heat fluxes

To illustrate how turbulent fluxes arise first we consider only electrostatic perturbations. The potential perturbation $\hat{\Phi}$ corresponds to a perturbed drift velocity $\hat{\mathbf{v}}_d = \mathbf{b}\times\nabla\hat{\Phi}/B$ producing an ambipolar particle flow. The flux surface average of this flow gives the particle flux Γ_a [8], which can be expressed as

$$\Gamma_a = \Re\langle \hat{n}_a \hat{\mathbf{v}}_d^* \cdot \hat{r}\rangle_\psi, \quad (4.15)$$

where $\hat{n}_a$ is the perturbed density and $\hat{r}$ is the radial unit vector. In the electrostatic case the drive term in the gyrokinetic equation [the right hand side of Eqs. (4.6) or (4.14)] is proportional to the potential perturbation, therefore the density or temperature perturbations that are different moments of the perturbed distribution function should also have this property.

Using that $(\mathbf{b} \times \nabla \hat{\Phi}^*) \cdot \hat{r} = i k_\theta \hat{\Phi}^*$, the particle flux can be written as

$$\Gamma_a = -\left\langle \frac{k_\theta T_a n_a}{eB} \left| \frac{e\hat{\Phi}}{T_a} \right|^2 \Im \left[\frac{\hat{n}_a / n_a}{e\hat{\Phi}/T_a} \right] \right\rangle_\psi , \tag{4.16}$$

where $(\hat{n}_a/n_a)/(e\hat{\Phi}/T_a)$ is called the density response. Similarly one finds that the energy flux is

$$Q_a = -\left\langle \frac{k_\theta T_a^2 n_a}{eB} \left| \frac{e\hat{\Phi}}{T_a} \right|^2 \Im \left[\frac{\hat{T}_a / T_a}{e\hat{\Phi}/T_a} \right] \right\rangle_\psi , \tag{4.17}$$

with the temperature response $(\hat{T}_a/T_a)/(e\hat{\Phi}/T_a)$. It is important to emphasize that – as it is clear from Eqs. (4.16) and (4.17) – particle (energy) fluxes rise only when the perturbed density (temperature) and the perturbed potential are out of phase. In particular if the non-adiabatic electron response is neglected there is no particle flux in a plasma without impurities. Trivially, the adiabatic part of the distribution does not lead to radial fluxes.

The mechanism of the quasilinear fluxes is illustrated in Fig. 4.1, where the potential is color coded and the density is contour-plotted with dotted lines. Particles drift along equipotential contours (indicated by blue arrows) with the $\mathbf{E} \times \mathbf{B}$ drift velocity. The mode propagates in the (electron or ion) diamagnetic direction (gray arrow), and the phase shift between the density and potential perturbations leads to that the the maxima of the density perturbations lag behind the maxima of the potential perturbations. And since the density is apparently higher in the outward (upward in the figure) than the inward flow region the resulting imbalance in the flows leads to a net radial particle flux. The same picture holds for temperature perturbations and energy fluxes.

The magnitude of the fluxes depends on the amplitude of the potential perturbations which remains undetermined in the solution of the linear problem. The most reliable method to calculate absolute fluxes is to perform nonlinear simulations, where nonlinear saturation mechanisms set the magnitude of the perturbed quantities. A less accurate, but computationally less expensive (and sometimes even analytically tractable) method is the quasilinear approach. In this case the linear problem is solved for different toroidal mode numbers to obtain the linear responses, then the fluxes are calculated using certain estimates for the magnitude of the perturbed potential based on simple mixing-length arguments or

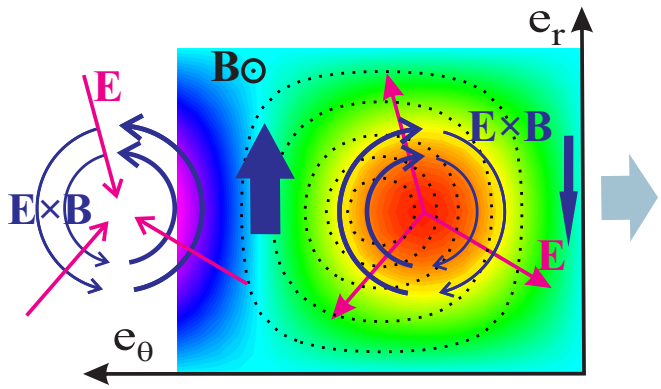

Figure 4.1: Schematic picture on the mechanism behind the radial fluxes driven by electrostatic turbulence. The perturbed potential – giving rise to $\mathbf{E} \times \mathbf{B}$ flows – is color density plotted; the perturbed density is contour plotted with dotted lines.

experience with nonlinear simulations. In analytical models usually only one representative linear mode is chosen (corresponding to the highest γ or $\gamma/k_\perp^2$). This approach is useful when the cross-phases between the perturbed quantities are approximately preserved as one moves from linear to non-linear simulations (the relevance of linear cross-phases is discussed in Ref. [38]).

Not only electrostatic, but magnetic perturbations can also drive particle and energy fluxes. In the notation of Eqs. (4.6) and (4.7), Eq. (4.15) can be written in terms of functions of the guiding center position as

$$\Gamma_a = \Re \left\langle \int d^3v H_a \langle \hat{\mathbf{v}}_d^* \rangle_\varphi \cdot \hat{r} \right\rangle_\psi , \tag{4.18}$$

where H_a is determined by the *electrostatic* gyrokinetic equation and $\langle \hat{\mathbf{v}}_d^* \rangle_\varphi = \mathbf{b} \times \langle \hat{\Phi}^* \rangle_\varphi / B$. In the electromagnetic case H_a is determined by Eq. (4.6) with a source term including the contributions from $\mathbf{v} \cdot \hat{\mathbf{A}}$, and $\langle \hat{\mathbf{v}}_d^* \rangle_\varphi = \mathbf{b} \times \hat{U}^* / B$.

4.4 Microinstabilities

The generation of fine-scale turbulence in plasmas is believed to be produced by microinstabilities [40, 41], i.e. instabilities which have wavelengths that are comparable to the ion or electron Larmor radii. To

obtain an overall picture of turbulent transport, and for the calculation of turbulence saturation levels, nonlinear processes have to be taken into account. However it is useful to identify the possible drives and conditions of turbulent processes. Investigation of linear mode characteristics can provide estimates of stability thresholds and parametric dependences of turbulent fluxes.

Since the goal of fusion experiments is to sustain enormous temperature gradients (the $\sim 4\,\mathrm{K} \approx 4 \cdot 10^{-4}$ eV cryostat of a superconducting device is separated from the ~ 10 keV plasma core only by a few meters or less), the plasma is always far from thermodynamic equilibrium. In this non-equilibrium state the available free energy might be transferred to turbulent flows via instabilities. Drift waves are particularly important class of microinstabilities which have often been invoked as the main source of plasma turbulence. Dissipation through, e.g., collisions or kinetic resonances often plays an important role in the de-stabilization of the drift waves. We mainly focus on these type of instabilities classified as *dissipative* modes, while some others, the *reactive* ones, do not require dissipation – similarly to a wide range of MHD instabilities. A quite important class of instabilities is predominantly *electrostatic*, although in spherical tokamaks and in the core of conventional tokamaks, where the kinetic pressure normalized to the magnetic pressure $\beta = p/(B^2/2\mu_0)$ is not negligibly small, *electromagnetic modes* might also play role [41]. In the present thesis we restrict our studies to electrostatic microinstabilities.

The microinstabilities have spatial scales that are typically much longer than the Debye length, in addition, they are slow instabilities compared to the plasma waves, so that the quasineutrality $\sum_\alpha e_\alpha \hat{n}_\alpha$ can be shown to be a very good approximation. The quasineutrality condition can be used to obtain a dispersion relation from the density responses of the different species.

The spatial and frequency scales of the microinstabilities that are thought to be accountable for the turbulence are indicated in Fig. 4.2 together with MHD and cyclotron waves. Clearly, the microinstabilities have much lower frequencies than the cyclotron frequencies (ω_{ce}, ω_{ci}), which allows for the use of gyro-averaged equations. The wavelengths are $10 - 10^4$ times smaller than the size of the system, ranging from ~ 10 times the ion Larmor radius to the electron Larmor radius. In contrast to the MHD waves, this feature makes them somewhat less sensitive to the shaping effects of the geometry, thus analytical calculations often rely

on the framework of a circular cross section, large aspect ratio model.

The ion temperature gradient (ITG) mode driven by ion magnetic drift and transit resonances, which is recognized as the most important drive of turbulence (to be discussed in detail in Sec. 4.4.1 [11–13]), is characterized by $k_\theta \rho_i \lesssim 1$, but since the turbulent energy flux spectra usually peak at lower wave numbers ($k_\theta \rho_i \sim 0.2 - 0.4$), an expansion in the FLR parameter might be appropriate. The trapped electron mode (TE or TEM, see Sec. 4.4.2 [14–16]), appearing in the same wave number range $k_\theta \rho_i \lesssim 1$, is destabilized by electron magnetic drift resonances or collisional dissipation. The TE and ITG modes have a frequency range between the ion and electron bounce frequencies (ω_{bi}, ω_{be}) which are comparable with the corresponding transit frequencies (ω_{ti}, ω_{te}). This means that the trapped electrons bounce several times during a wave period; thus usually a bounce averaged electron gyrokinetic equation is used, in which the parallel streaming term ($v_\parallel \mathbf{b} \cdot \nabla$) is annihilated by the averaging operation. Trapping effects become important when the mode frequency is comparable to or lower than the bounce frequency, since then the particles are moving quickly enough along the field lines to sample the whole toroidal geometry during a mode period. Whereas for electron temperature gradient (ETG) and ITG modes the frequencies are higher than the electron/ion bounce frequencies, respectively. The corresponding trapped particle modes, namely, the trapped electron mode and the trapped ion mode (TIM) [42], have frequencies that are lower than or comparable to the bounce frequencies, as it can be seen in Fig. 4.2. Since the bounce frequency of trapped ions is usually smaller than the ITG mode frequency, the ion trapping is often neglected in ITG studies [43].

As an illustration of the drift wave phenomenon, from the quasineutrality condition one can derive the simplest possible electrostatic drift wave by assuming adiabatic electron response, and deriving the ion response from Eq. (4.14), neglecting the FLR effects ($J_0(z_i \to 0) \to 1$) and all the terms on the left hand side, except $-i\omega g_i$. This wave has the frequency $\omega = \omega_{*e}$. It is marginally stable since $\Im(\omega) = 0$, and it propagates on the flux surface in the electron diamagnetic direction. Since the magnetic curvature is neglected, $\omega_{Di} = 0$, this mode does not rely on the toroidal geometry: it is a slab mode. The first term of Eq. (4.14) coming from the compressibility-like $v_\parallel \mathbf{b} \cdot \nabla$ term of Eq. (4.6) would give sound wave propagation along the field lines. Neglecting this term would mean that the ion inertia is assumed to be infinite, which is

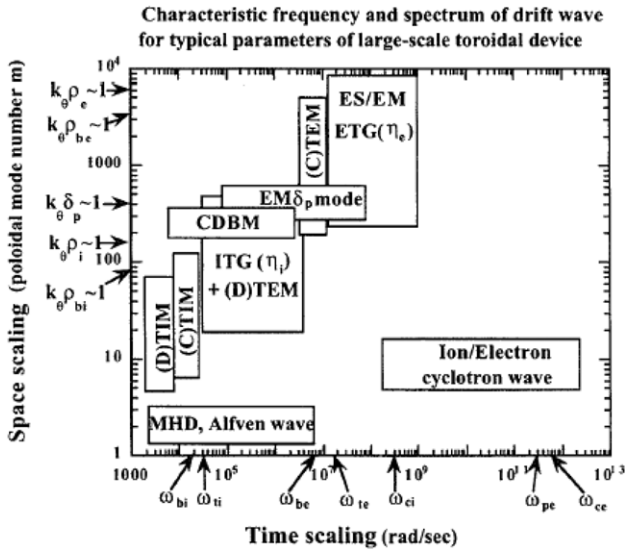

Figure 4.2: Typical spatial and temporal scales of different microinstabilities. TIM – trapped ion mode, TEM – trapped electron mode, ITG (η_i) – ion temperature gradient mode, ETG (η_i) – electron temperature gradient mode, CDBM – current diffusive ballooning mode, δ_p – skin-depth (mode); (D) – dissipative, (C) – collisionless, ES/EM – electrostatic/electromagnetic. [Source: *J. Plasma Fusion Res.* **76**, 1280 (2000)]

justified if the parallel phase velocity of the wave is much higher than the ion thermal velocity and the magnetic field is not strongly sheared. In the toroidal picture, this term might be neglected if the considered frequency range is much higher than the transit or bounce frequency of ions. Since $\rho_e \ll \rho_i$, in the description of ion modes ($k_\theta \rho_i \sim 1$) the electron FLR effects can always be neglected (drift kinetic electrons are considered).

In a local analysis of the ion response, taking collisions into account by a simple energy-dependent Krook model $C[g_i] = -(\nu/x^3)g_i$, and replacing the parallel compressibility term by $k_\parallel v_\parallel$, the ion gyrokinetic equation reduces to an algebraic equation with the solution

$$g_i = \frac{e f_{i0}}{T_i} \frac{\omega - \omega_{*i}\left[1 - \left(\frac{3}{2} - x^2\right)\eta_i\right]}{\omega - k_\parallel v_\parallel - \omega_{DT}(x_\perp^2/2 + x_\parallel^2) + i\nu/x^3} J_0(z_i)\phi, \qquad (4.19)$$

where $x = v/v_{Ti}$ and $\omega_{DT} = \omega_{Di} v_{Ti}^2/(v_\perp^2/2 + v_\parallel^2)$. We have introduced

$\eta_i = L_n/L_T$, which is a crucial parameter in ITG theory [41], and we have taken the strongly ballooning limit $\theta \to 0$. The ion density response appearing in the dispersion relation is the velocity integral of this expression transformed back from guiding center to real space [by a multiplication with $J_0(z_i)$]. The integral contains poles coming from the resonances in the denominator. These terms - the transit, the magnetic drift, and collisional resonances – can destabilize the mode. Depending on whether the first or the second of these resonances dominate the resulting instability is called slab or toroidal ITG mode, respectively. We note that in tokamak core plasmas the toroidal mode is the dominant. If all resonances and FLR effects are neglected (as in the previous example) the $(3/2)\eta_i$ and $x^2\eta_i$ terms in the numerator cancel out in the velocity integration and the mode is not affected by temperature gradients.

In general, the collision term contains a differential operator in velocity space and the parallel ion dynamics term makes the problem a differential equation in real space. Moreover, considering the full dispersion relation with a bounce-averaged electron response term, one obtains an integro-differential equation in phase space, which would be intractable analytically without further approximations. One can make use, for example, of the following considerations: If $\nu_e/\omega \lesssim 1$, then ν_i/ω is negligibly small. For $\omega_{bi} \ll \omega_{DT}$ the parallel dynamics term is much smaller than the magnetic drift term $k_\parallel v_\parallel \ll \omega_{DT}$. In addition, if the wavelength is comparable to or longer than the ion gyro-radius, the electron finite Larmor radius corrections can be neglected $z_i \lesssim 1 \Rightarrow z_e \sim 0$. Furthermore, one can try to identify the terms that shape the mode structure, and others setting the mode frequency. Additionally, if $\omega \ll \omega_{be}$ the parallel dynamics dominates the circulating electron response; these electrons can almost freely follow the potential perturbation and therefore have a Boltzmann response. If the drift frequency for thermal velocities, ω_{DT}, is much lower than the mode frequency, the drift resonance is expected to play minor role. Then the expansion of the integrand in the smallness of ω_{DT}/ω – the so called "non-resonant expansion" – might be useful, but the validity of this approximation turns out to be limited [44].

4.4.1 Ion temperature gradient mode

The most important microinstability affecting the ion thermal confinement is the ion temperature gradient mode (ITG or η_i-mode), which is a passing particle mode in the $k_\parallel v_{Ti} \ll \omega \ll k_\parallel v_{Te}$ frequency range. Clas-

sically the mode was investigated assuming adiabatic electron response and the ion response was calculated as (4.19). Depending on whether the mode is destabilized by the $k_\parallel v_\parallel$ or the ω_{Di} resonance the mode is called slab- or toroidal ITG. The former mode, which is basically a coupled drift wave/ion acoustic wave in the presence of a radial ion pressure gradient, appears even if we neglect the magnetic curvature. Its typical frequency can be estimated as $\omega \sim \left(k_\parallel^2 v_{Ti}^2 \omega_{*i} \eta_i\right)^{1/3}$ and it propagates in the ion diamagnetic direction [41].

In toroidal geometry the curvature replaces the acoustic wave as the main driving mechanism. The quasi-neutrality condition leads to an eigenfunction problem in the ballooning angle with solutions peaking near $\theta = 0$, i.e., in the bad-curvature region, thus showing a "ballooning structure". In this region, the magnetic drift acts to destabilize the mode through the ion temperature gradient [41]. The transit resonance term and the FLR effects also play an important role in shaping the ballooning eigenfunction. This mode also propagates in the ion diamagnetic direction and has a frequency approximately $\omega \sim (\omega_{*i}\omega_{Di}\eta_i)^{1/2}$.

The physical mechanism behind the toroidal ITG mode is the following. If there is a temperature perturbation in the plasma on the outboard side of the torus, the (mainly vertical) magnetic drift of particles will have different velocities in the lower and higher temperature regions, which leads to a growing density perturbation that is out of phase with the temperature perturbation. The density perturbation generates a potential perturbation, which, in turn, will generate $\mathbf{E} \times \mathbf{B}$ flows. The phase of the perturbed flows with regard to the temperature perturbations is such that they convect hot plasma to the already higher temperature spots of the temperature perturbation, leading to the growth of the perturbation amplitude. On the inboard side the relative direction of ∇T is the opposite of ∇B and the magnetic curvature, and the ITG instability is stabilized (thus we often refer to the outboard and inboard sides of the torus as unfavorable and favorable curvature regions). The poloidal angle dependence of the drive and the FLR stabilization shapes the typical "ballooning" form of the mode structure.

An important feature of the ITG mode which appears in both slab and toroidal cases is that the mode is stable below a critical temperature gradient threshold, as illustrated in Fig. 4.3.

Within the adiabatic electron approximation and for pure hydrogen plasma, the mode has no unstable roots for $\eta_i = 0$. Retaining parallel ion dynamics is found to be stabilizing through Landau damping, which thus

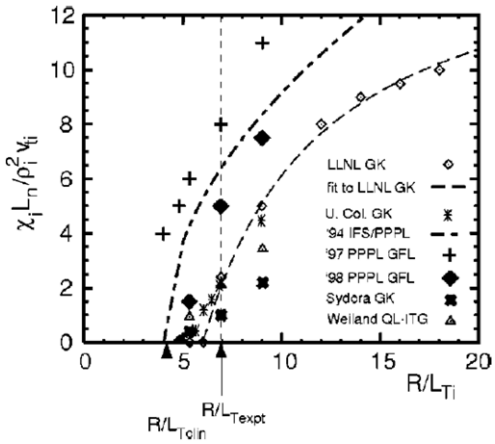

Figure 4.3: Ion heat diffusivity as a function of the logarithmic temperature gradient calculated with different gyro-kinetic and gyro-fluid codes. [Source: *Phys Plasmas* **7**, 969 (2000)]

introduces a q dependence, since in tokamaks the parallel wavelength is comparable to the connection length $\sim Rq$ [45]. Introducing a non-adiabatic trapped electron response, a new root, the trapped electron mode appears which can be clearly distinguished from the ITG mode if η_i, η_e and the trapped electron fraction are high, although there are parameter regimes where the two modes form a single hybrid mode [46], which can be unstable for η_i values lower than the classical threshold value (unstable modes with $\eta_i = 0$ are possible in case of impure plasma as well). For toroidal ITG the relevant parameters are R/L_n and R/L_T instead of η_i and $\epsilon_n = L_n/R$.

We note that the slab mode can be relevant in toroidal geometry as well, when the magnetic drift frequency becomes much smaller than the diamagnetic frequency (when ϵ_n is small), which is typical in the edge region, where the density profile is not flat [8].

Turbulent fluctuations can generate zero toroidal and poloidal mode number perturbations which are then not damped by Landau-damping. These, so called zonal-flows [47], appear as predominantly poloidal flows within flux surfaces; the direction of which varies on a radial scale comparable to the ion Larmor radius.

Zonal flows, together with neoclassical equilibrium flows, have a strong linear stabilizing effect [48]. In addition, the radial correlation

length of turbulent structures is decreased by the flows, which leads to reduced transport for a given fluctuation level. This double effect is shown in Fig. 4.3 where the ion heat diffusivity curve showing higher threshold corresponds to higher $\mathbf{E} \times \mathbf{B}$ shearing rate. This kind of turbulence suppression is recognized to be important for the non-linear self regulation of the plasma and transport barrier formation.

4.4.2 Trapped electron mode

The magnetic field strength in tokamaks decreases from the inboard side of the torus ("high field side" or HFS) towards the outboard side ("low field side" or LFS) approximately as $1/R$. Thus the gyrating particles – behaving like small magnetic dipoles following the field lines – experience a magnetic mirror force. An $\mathcal{O}(\sqrt{\epsilon})$ fraction of particles with parallel velocity at the outboard mid-plane lower than $v_\perp \sqrt{B_{max}/B_{min} - 1}$ is reflected back from the high-field region, bouncing back and forth. These *trapped particles* spend most of their time in the bad-curvature region, the LFS, thus the curvature drift has a preferred direction (while this effect averages out for the circulating particles), and the associated local electrostatic fields drive $\mathbf{E} \times \mathbf{B}$ drifts giving rise to micro-scale instabilities. The trapped particles cannot follow the electrostatic perturbations freely even if their inertia is negligibly small (mathematically: the $v_\parallel \mathbf{b} \cdot \nabla$ term vanishes on average over the trapped orbits), therefore they behave non-adiabatically.

If collisions are not too frequent to de-trap the trapped particles under a bounce period, various kinds of trapped particle instabilities can arise. On the other hand, the collisional de-trapping can turn non-adiabatic particles to adiabatic [49]. Therefore collisions play a crucial role in the theory of trapped particle instabilities. The collision frequency ν is usually defined by the frequency of $\pi/2$ angle scattering. It is however convenient to define a higher, *effective collision frequency* $\nu_{\text{eff}} = \nu/\epsilon$ describing the frequency of collisional de-trapping.

The trapped electron mode is one of the most important microinstabilities which can dominate the transport in the presence of internal transport barriers and certainly significantly contributes to the anomalous fluxes in tokamaks [40]. The *dissipative TEM* is destabilized by the combined effect of the electron temperature gradient and the collisions. The response of the circulating particles is dominated by the parallel dynamics due to the small electron inertia, therefore neglecting the $\mathcal{O}(\frac{\omega}{k_\parallel v_{Te}}) \ll 1$ non-adiabatic circulating electron response can

be adequate [16] in the electrostatic case. For even lower collisionalities the electron magnetic drift frequency resonance destabilizes the mode, which is then called the *collisionless TEM*.

The maximum growth rate typically occurs at $k_\theta \rho_i \lesssim 1$. For high collisionalities the growth rate γ varies approximately as $1/\nu$. The TEM stability boundary shows a strong dependence on collisionality and the FLR parameter [16].

In paper D we study electron cyclotron (EC) heated and ohmic (OH) plasmas from the T10 tokamak, where the transport is found to be mainly driven by trapped electron modes. The qualitatively different scaling with the electron-to-ion temperature ratios in the two cases is due to that the TE mode is driven mainly by electron temperature gradients in the EC case and density gradients in the OH case. Collisional stabilization of the TE modes is also found to be important in these experimental scenarios.

4.5 The role of collisions in turbulent transport

In the absence of microinstabilities the particle and heat fluxes across the magnetic surfaces are determined by collisional transport processes, as it was discussed in Sec. 3. Since collisional dissipation affects the non-adiabatic response of the particles it plays an important role in the turbulent transport as well.

In gases collisions change the velocity of an atom almost instantaneously, so that its trajectory in phase space is a continuous set of line segments. In plasmas, on the other hand, each particle is in a continuously running Coulomb interaction with a large number of other particles being closer than a few Debye lengths. Since small-angle scattering dominates, the phase-space trajectory of a single particle is a smooth curve, and the collision operator – describing the variation of the distribution function due to collisions – can be expressed as the $\Delta t \to 0$ limit of

$$C\left[f(\mathbf{v},t)\right] = -\nabla_{\mathbf{v}}\left(\frac{\langle \Delta \mathbf{v}\rangle}{\Delta t} f\right) + \nabla_{\mathbf{v}}\nabla_{\mathbf{v}} : \left(\frac{\langle \Delta \mathbf{v}\Delta \mathbf{v}\rangle}{2\Delta t} f\right) + \ldots, \quad (4.20)$$

where the expectation value is denoted by angle bracket. The first term in Eq. (4.20) is responsible for the collisional drag on the particle while the second term describes diffusion in velocity space.

The $\langle \Delta v_i \rangle$ and $\langle \Delta v_i \Delta v_j \rangle$ quantities can be calculated by a statistical description of binary Coulomb collisions between plasma particles. The

$\int dr/r$-like integral over the possible impact parameters do not need to be evaluated over an infinite range, since the particles being outside the Debye sphere do not contribute to the integral and the smallest distance between the colliding particles $r_{\min}$ is also finite. So the integration limits are to be cut off at λ_D and $r_{\min}$, which leads to the appearance of the *Coulomb logarithm* parameter $\ln\Lambda = \ln(\lambda_D/r_{\min})$ in the collision frequency.

A plasma particle is in a continuously running Coulomb interaction with a large number of other particles, and the small-angle scattering events strongly dominate, so the quantities, such as *mean-free path* or *collision time* from the classical picture of collisions are to be reconsidered in this context. The collision time τ is defined as the time which is required for an order unity relative change in the velocity of the particle as a result of the cumulated effect of Coulomb interactions. Then the collision frequency is defined as $\nu = 1/\tau$.

The electron-ion collision frequency depends on electron mass m_e, electron temperature T_e, ion density n_i and ion charge Z in the following manner [27]

$$\nu_{ei} \propto \frac{e^4 n_i Z^2 \ln\Lambda}{\epsilon_0^2 m_e^{1/2} T_e^{3/2}}. \tag{4.21}$$

Since ν_{ei} is independent of m_i, the total electron-ion collision frequency in the presence of several ion species can be conveniently written as $Z_{\text{eff}}\nu_{ei}(Z=1)$. Due to the high ion-to-electron mass ratio much higher number of elementary interactions is needed for an ion to significantly change its velocity as a result of collision by electrons than vice versa. Accordingly, the relative magnitudes of the different collision frequencies are $\nu_{ee} \sim \nu_{ei} = \nu_{ii}\sqrt{m_i/m_e} = \nu_{ie} m_i/m_e$ (considering singly charged ions).

Making use of Eq. (4.20), the most general collision operator describing binary collisions, the so-called Fokker-Planck operator [50] can be derived to be [51]

$$C_{ab}\left[f_a(\mathbf{v}), f_b(\mathbf{v}')\right] = -\frac{e_a^2 e_b^2 \ln\Lambda}{8\pi\epsilon_0^2 m_a^2} \times \partial_{v_k} \int \frac{u^2\delta_{kl} - u_k u_l}{u^3} \left(\frac{f_a(\mathbf{v})}{m_b} \partial_{v_l'} f_b(\mathbf{v}') - \frac{f_b(\mathbf{v}')}{m_a} \partial_{v_l} f_b(\mathbf{v}) \right) d^3v', \tag{4.22}$$

where $\mathbf{u} = \mathbf{v} - \mathbf{v}'$ is the relative velocity of the colliding particles and the indices a and b refer to the colliding species. In several cases it is

useful to derive an approximate, model collision operator that is simpler, and therefore less accurate than the one given above, but still models the physical phenomena that are important for the problem. It is always required that the collision operator drives the system towards local thermodynamic equilibrium. In particular, if f_a and f_b are two Maxwellian distributions with equal temperatures and mean velocities the operator should vanish.

Since electrons are much lighter than ions, the dominant process in the electron-ion collisions is pitch-angle scattering, driving a velocity diffusion on a constant-energy surface. This process tends to make the electron distribution isotropic in the ion rest frame. The energy transfer is small due to the high ion-to-electron mass ratio m_i/m_e, so the electron speed is approximately conserved. Furthermore, if the gyro-angle dependence of the collisions can be neglected the collision operator reduces to the pitch-angle scattering operator

$$C_{ei} \approx \frac{\nu_{ei}}{x_e^3}\mathcal{L} \equiv \frac{\nu_{ei}}{x_e^3}\frac{1}{2}\partial_\xi\left(1-\xi^2\right)\partial_\xi, \tag{4.23}$$

where $\xi = \cos\theta$ with the pitch-angle θ.

If one wants to investigate the collisional de-trapping of trapped electrons, it is sometimes enough to keep only a pitch-angle scattering model operator of electron-ion collisions since trapping depends only on the cosine of the pitch angle, $\xi = v_\parallel/v$. In other cases it is merely sufficient that the collision operator drives the particle distribution towards a Maxwellian, so that it reduces the perturbed part of the distribution. An example of such an operator is the so-called *Krook model*, $C = -\nu(f_a - f_{Ma})$, where an energy dependence can be included in the collision frequency ν. For other applications it can be important that the collision model conserves energy and momentum, or that it incorporates other physical effects, such as parallel velocity diffusion. A systematic derivation of model collision operators is given by Hirshman and Sigmar [52].

It was found both experimentally and in simulations that collisions can strongly affect anomalous particle transport [53]. Electron density profiles in tokamak cores are usually not completely flat, although the particle sources are mainly localized in the periphery of the plasma. Neoclassical theory predicts an inward particle transport, due to the Ware pinch [54]. However this effect is often not sufficiently strong to explain the experimentally found density peaking, which implies the existence of an anomalous component of the particle pinch. Experimentally, density

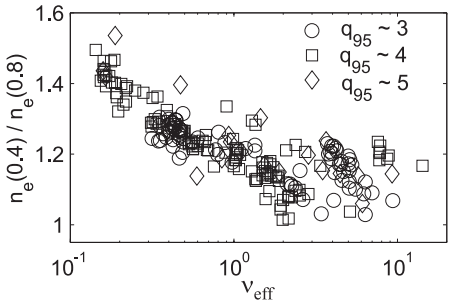

Figure 4.4: Density peaking parameter as a function of effective collisionality, measured in H-mode plasmas of the ASDEX-Upgrade tokamak for three different values of the edge safety factor q_{95}. [Source: *Phys. Rev. Lett.* **90**, 205003 (2003)]

peaking is found to increase with decreasing collisionality [53, 55–57] for a wide range of plasma parameters, as shown in Fig. 4.4. Since fusion power scales as n^2, this phenomenon is crucial for reactor relevant fusion experiments operating with high temperatures and thus having low collisionalities.

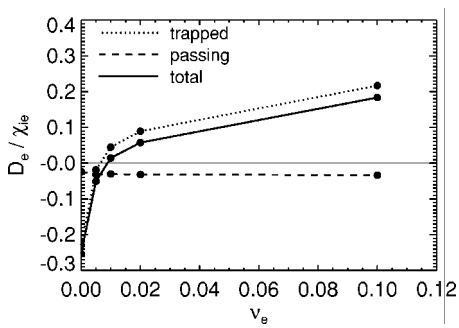

Figure 4.5: Normalized electron particle flow as a function of electron collision frequency (ν_e is normalized to c_s/a). [Source: *Phys. Plasmas* **12**, 022305 (2005)]

If collisions are neglected, the inward particle fluxes can be explained by gyrokinetic theory [58]. The transport is dominated by ITG driven turbulence in most cases, and ITG modes produce an inward particle flux through magnetic curvature effects and thermodiffusion, as predicted by both linear theory and nonlinear gyrokinetic simulations [44]. In

fact, the particle flux shows a very strong collisionality dependence for low collision frequencies as illustrated in Fig. 4.5; showing the result of nonlinear gyrokinetic simulations using a pitch-angle scattering collision operator. We note that gyro-fluid simulations predict somewhat higher collisionality for the reversal of particle flows [59].

The collisionality dependence of the particle flux at low electron-ion collision frequencies suggest that the non-adiabatic electron response is affected (note that $\Gamma \propto \Im(\hat{n}_e)$ and $\nu_i \approx 0$). The circulating electrons are expected to have a quite weak non-adiabatic response which is almost independent of collisionality [44]. This conclusion is supported by Fig. 4.5, where the trapped and passing contributions in the particle flux are also indicated. The $\sqrt{\nu_{ei}}$-like collisionality dependence can be interpreted with the development of a boundary-layer at the trapped-passing boundary.

After discussing the effect of electron-ion collisions on microinstabilities and transport we note that ion-ion collisions also play a role in turbulent transport by providing the main stabilization mechanism of zonal-flows, thus affecting the saturated level of transport.

In paper A we investigate the collisionality dependence of the quasi-linear particle flux for weakly collisional plasmas using a WKB (Wentzel–Kramers–Brillouin) solution of the electron gyrokinetic equation, where the electron-ion collisions are modeled by the pitch-angle scattering operator. While in this work the mode frequencies are constant input parameters, in paper B we take collisional effects into account through the dispersion relation as well. In this extended model the density responses are calculated without assuming the magnetic drift frequency to be small.

4.6 Nonlinear simulations and transport analysis

As it has been established, linear gyrokinetic simulations consider only one exponentially growing toroidal mode which, in the absence of nonlinear mode coupling mechanisms, never saturates. Accordingly, a linear simulations does not provide the magnitude of the perturbed quantities, and the absolute level of the transport, in contrast to nonlinear simulations. Thus, in order to quantitatively compute turbulent transport one has to resort to nonlinear simulations.

There are different approaches to solve the nonlinear gyrokinetic-

Maxwell system and different levels of sophistication implemented in nonlinear codes. The "delta-f" codes separate the lowest order (equilibrium) distribution and solve only for the next order deviation from the equilibrium. The "full-f" codes solve for the whole distribution function to the same accuracy in ρ_*. Since there is no full-f formalism to handle collisions, the full-f approach has no significant advantage compared to the delta-f approach. The continuum models evolve the discretized 5-D phase space distribution according to the gyrokinetic equations, while the particle-in-cell codes sample the phase space through a large number of quasi-particles and follow their trajectories under the effect of their self-consistently generated electromagnetic fields.

All of these methods are solved in an initial value manner. After the exponential growth of linear modes the fluctuations reach an amplitude where nonlinear mode couplings become important, until the system evolves to a fully developed turbulence, where the initial conditions become unimportant (in a statistical sense). Then the simulation is run for a sufficiently long time in this phase until the statistical properties of the desired quantities, such as radial fluxes, are adequate; see an illustration in Fig. 4.6.

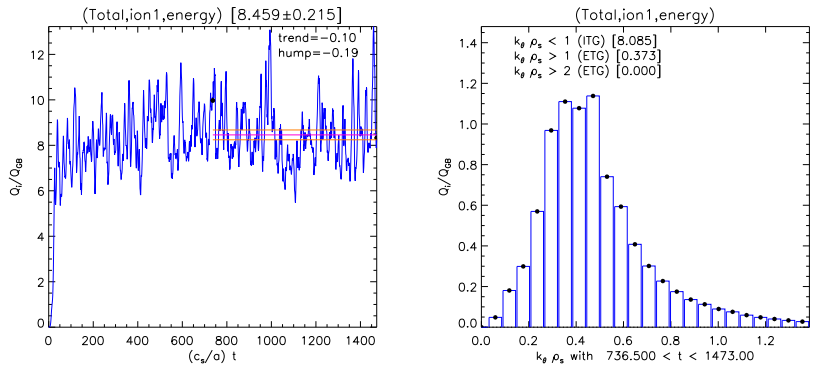

Figure 4.6: Results of a nonlinear GYRO simulation for the local parameters of a DIII-D discharge. Left: Time trace of the ion energy flux (given in gyro-Bohm units), Right: poloidal wave number spectrum (at the outboard-midplane) of the ion energy flux, averaged over the half of the total simulation time.

Exploiting the elongated nature of the turbulent fluctuations in tokamaks gyrokinetic simulation codes use conveniently chosen field aligned coordinate systems. These are rather similar to the ballooning coordi-

nates, however they are more fitted to handle the $\mathbf{E} \times \mathbf{B}$ nonlinearity and zonal flows. The simulation domain is a "flux tube" that has a radial and binormal extent that is significantly larger than the correlation length in these directions ($\sim 10\rho_i$), and follows the field lines over a few connection lengths (again, depending on the parallel correlation length of the turbulence).

In the limit of vanishing ρ_* (that is relevant to large tokamaks, such as ITER) the plasma parameter profiles and their derivatives can be approximated by constant values over the perpendicular simulation domain. Since the perpendicular domain size is chosen to be larger than the perpendicular correlation length, periodic boundary conditions can be applied to increase numerical efficiency. But sometimes, when profile variations and non-local effects are expected to play a role in the considered problem, the periodic boundary conditions and the profile-flattening can be relaxed (these are called "global" simulations).

The existing gyrokinetic simulations do not model the time evolution of the background profiles as these being a higher order effect in the ρ_* expansion, but rather evaluate the radial transport in a particular instant of time at a certain radial location. To quantitatively calculate the energy and particle fluxes the profiles should be known with quite high accuracy, since the fluxes often exhibit a strong nonlinear dependence on the gradients of plasma parameters [60]; changing the gradients by a small amount can lead to significant differences in the fluxes. When drift-wave turbulence models are validated to experiments, instead of calculating the "fixed gradient" fluxes, it is sometimes more convenient to calculate how the profiles should look like to produce the experimental level of fluxes (the latter can be calculated from power balance if the energy deposition profiles are given). This can be done by iteration schemes requiring a large number of evaluation of the transport in several radial locations [61].

Even one nonlinear gyrokinetic simulation with appropriate phase-space resolution requires considerable computational resources, therefore it is clear that predictive profile calculations are extraordinarily expensive. This shows the advantage of gyro-fluid and/or quasilinear models (e.g. TGLF [62] and the Weiland model [8]) that – although not being as accurate – can calculate the turbulent fluxes much faster than nonlinear gyrokinetic codes.

In larger devices the perpendicular spatial scale of the turbulence is unaffected by the system size and it is mainly linked to the ion Larmor

radius ρ_i, while the typical frequencies of $k_\theta \rho_i \sim 1$ fluctuations scale as v_{Ti}/a. From this picture – purely based on dimensional arguments – we expect that the diffusivities should follow gyro-Bohm scaling, that is $\chi \sim \rho_i^2 v_{Ti}/a$. The theoretically predicted gyro-Bohm scaling is in conflict with the experimentally usually observed improving confinement with increasing isotope mass. In paper E we study the effect of the primary ion species of differing mass and charge on instabilities and transport through first principles gyrokinetic simulations with GYRO. We also present the transport analysis of three balanced beam injection DIII-D discharges having different main ion species: deuterium, hydrogen and helium.

Chapter 5

Beam emission spectroscopy

The progress in the understanding of anomalous transport, such as the development of plasma turbulence models, strongly rely on experimental data measured by various kinds of plasma diagnostic tools. Since in such high temperature systems, the methods based on physical contact of the measuring device and the plasma are quite limited, the diagnostics either passively collect radiation or particles emitted by the plasma (*passive diagnostics*), or observe the interaction of the plasma with some material/radiation introduced externally (*active diagnostics*) [63]. Beam emission spectroscopy (BES) is an important, widely used active diagnostic tool of fusion plasmas, which is based on the observation of light emitted by a high energy neutral beam injected into the plasma [64]. The measured intensity distribution corresponding to the spontaneous emission from the highest population excited atomic state, the *light profile*, provides information on the distribution of plasma parameters affecting the beam evolution.

Heating beams (neutral beam injection, NBI) – observed tangentially to the magnetic field lines – are also used for beam emission spectroscopy [65,66], although in the thesis we focus on beams used only for diagnostic purposes [67–70]. The diagnostic beams have much lower beam current ($\sim$ mA) than the NBI beams, and due to the attenuation of the beam in the plasma, mainly the outer plasma regions can be probed by them. Since the density of beam atoms is $\sim 10^{14}$ m^{-3} (which is low compared to $\sim 10^{19}-10^{20}$ m^{-3} plasma densities), the momentum transfer from the beam is negligibly small, and the quantity of deposited beam material is

usually too low to noticeably modify the Z_{eff} in the plasma, the method is considered to be non-intrusive [71]. A further advantage of BES is that it is not line integrated, but a well localized measurement of plasma parameters.

The electron density, the temperature of plasma particle species (mainly T_e) and the distribution of impurities are the relevant parameters determining the beam evolution [72]. Due to the relatively weak temperature dependence of the reaction rates of alkali elements, they are well suited for electron density measurements. We restrict our studies to the prevailing alkali beam emission spectroscopy.

One of the main purposes of alkali BES is the electron density fluctuation measurement [67, 69] (with $\gtrsim 0.5$ μs temporal resolution [31]) which provides useful – statistical or time-resolved – information on turbulence, such as frequency-, wave-number spectra, flow velocities, spatial and temporal correlations, or even snapshots of the turbulence. In fluctuation measurements linear – but not local – response in emitted intensity to density perturbations is assumed, which depends on the equilibrium density profile. The time resolution of such measurements is limited by the photon statistics which depends on the achievable beam current and the efficiency of the observation. Results of BES fluctuation measurements are shown in Fig. 5.1, where – in the left figure – the broadband turbulent spectrum and the dramatic reduction of the density fluctuations in an L-H transition is plotted, and in the right figure the frequency spectrum of density fluctuations in different radial positions is shown.

An other important application of alkali BES is the electron density profile measurement [64, 68, 72]. This measurement, relying on the knowledge of the derivative of the light profile, requires smooth, time averaged light profiles, which limits its time resolution. The spatial resolution of both measurement modes is limited by the characteristic distance covered by a beam atom under the spontaneous decay of the observed transition.

In NBI BES measurements the beam is wide enough to make 2-dimensional turbulence measurements possible for a fixed beam position. By means of scanning the beam, poloidally resolved measurements are also feasible with the $\sim 1-2$ cm wide diagnostic beams [67]. In these measurements, the scanning frequency is higher than the achievable sampling frequency of the profile measurements. In several cases the beam is observed from the same poloidal plane, and a time averaged

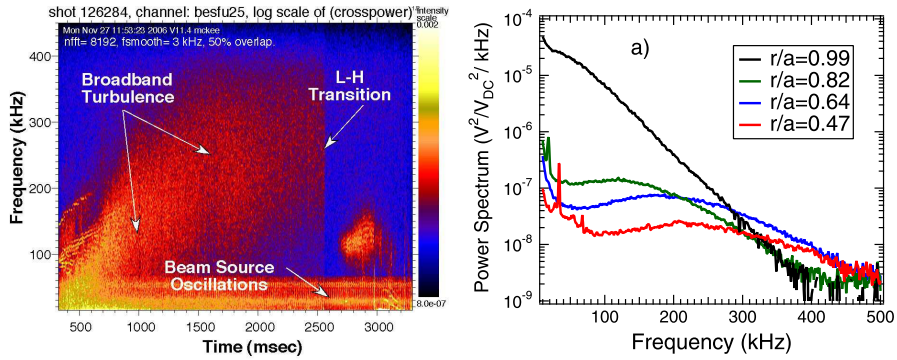

Figure 5.1: Deuterium BES measurement on the DIII-D tokamak. Left: spectrogram showing the evolution of turbulent density fluctuations in an L-H transition ($r/a = 0.65$). Right: Power spectra of fluctuations in different radial positions. [Source: *Plasma and Fusion Research* **2**, S1025 (2007)]

signal of the fluctuation measurement is used for calculating the density profile which is, in turn, used as an input to the evaluation of the fluctuation measurements. In this configuration, the density calculation is based on the light profile from a beam which is several times wider than the physical beam width. In spite of that, in many experiments a one-dimensional beam is considered in the density calculations.

The evolution of the beam in the plasma is accurately described by the *collisional radiative model* [73] which considers collisional and spontaneous atomic transitions. Each collisional process is characterized by a rate coefficient defined as

$$R = \int d^3v \sigma(|\mathbf{v} - \mathbf{v}_B|)\, |\mathbf{v} - \mathbf{v}_B|\, f_\alpha(\mathbf{v}), \tag{5.1}$$

where $\mathbf{v}_B$ is the velocity of the beam atoms, σ is the cross section of the process and f_α is the *velocity distribution* of the colliding species, considered to be a Maxwellian. The rate coefficients depend parametrically on the beam energy and the temperature T_α. In terms of the rate coefficients, the evolution of the occupation densities of the atomic states is described by the rate equations, which read in the rest frame

of beam atoms

$$d_t N_k = -N_k \sum_{j(<k)} A_{jk} + \sum_{j(>k)} A_{kj} N_j \tag{5.2}$$
$$+ \sum_{\alpha} n_\alpha \left\{ -N_k \left[R^{(\alpha)}_{+k} + \sum_{j(\neq k)} R^{(\alpha)}_{jk} \right] + \sum_{j(\neq k)} R^{(\alpha)}_{kj} N_j \right\},$$

where the different plasma species are indexed by α, and the j and k indices run over the different atomic levels; n denotes particle density, N is the population of an atomic state. A_{kj} is the spontaneous transition frequency and R_{kj} is the rate coefficient corresponding to the $j \to k$ transition. The ionized state is denoted by $+$, and the ionized beam atom is considered to be lost from the beam. In a simulation the evolution of a finite number of levels are followed, and the populations of the higher principal quantum number states are neglected. After approximations regarding the impurity content Eq. (5.2) can be written in the more compact form [72]

$$\frac{d\mathbf{N}}{dx} = [n_e(x)\mathbf{A}(x) + \mathbf{B}] \cdot \mathbf{N}, \tag{5.3}$$

where the different atomic populations are stored in the vector $\mathbf{N}(x)$ and the matrices $\mathbf{A}(x)$ and $\mathbf{B}$ describe collisional and spontaneous atomic transitions.

Observing the $\iota \to \varphi$ transition the emitted light intensity is proportional to $N_\iota J A_{\varphi\iota}/v_B$, where the J is the current density of the beam. Since in alkali BES measurements one spectral line is observed, the evolution of only one atomic population N_ι is known directly.

5.1 Turbulence measurements

In turbulence measurements it is assumed that the electron density distribution along the beam can be decomposed to a slowly varying density profile and a fluctuating density $n_e(x,t) = n_{e0}(x) + \hat{n}_e(x,t)$ [74]. The time average of $\hat{n}_e(x,t)$ vanishes, and on the time scale of fluctuations the profile is considered to be static. Here, for simplicity, we consider one dimensional fluctuation measurements and neglect the finite thickness of the beam, although the quantities to be introduced can be generalized to two dimensions.

The measured light profile S can be decomposed accordingly to a static and a fluctuating part $S(x,t) = \mathcal{S}\left[n_{\alpha 0}(x), T_{\alpha 0}(x)\right] + \hat{S}(n_\alpha, T_\alpha)$, where $\mathcal{S}$ can be determined by solving the rate equations (5.3), and the fluctuation part depends on both the static and fluctuating parts of plasma parameters. However, for alkali beams, the effect of temperature and impurity content fluctuations on $\hat{S}$ can be neglected. Then, the fluctuating part of the measured light profile can be written in terms of the density fluctuation transfer function $h(x, x')$ as

$$\hat{S}(x,t) = \int_0^x \hat{n}_e(x',t) h(x,x') dx', \tag{5.4}$$

where the transfer function is considered to be dependent only on the static part of the plasma parameter profiles. (In fact, the value of $\hat{S}(x,t)$ depends on the density fluctuations at the retarded time $t-(x-x')/v_B$, but in the present reasoning, this effect is neglected.) The transfer function is needed in the calculation of density fluctuation cross-correlations from light profile cross-correlations.

The transfer function can be easily calculated as

$$h(x, x_0) = \mathcal{S}\left[n_{e0} + \delta(x' - x_0)\right] - \mathcal{S}\left[n_{e0}\right], \tag{5.5}$$

in other words, an elementary fluctuation is superimposed on the density profile at point x_0, the difference appearing in the light profile is monitored. Eq. (5.5) reflects the importance of static density profiles in the evaluation of fluctuation measurements.

5.2 Electron density measurements

High spatial and temporal resolution electron density profile measurements [31, 68, 72] in the outer regions of fusion plasmas are of great importance, providing useful information on edge phenomena, such as pedestal formation and ELM activity. Also, as we pointed out, the knowledge of the density profile is also an important input to BES fluctuation measurements.

In the *direct problem* – such as in a BES measurement design – we are interested in the measured light profile given the plasma parameter profiles along the beam line. It consists of the simulation of beam evolution and the modeling of the observation of the emitted light. Considering an ideal (one dimensional) beam, the beam evolution can be calculated

by the numerical integration of the rate equation system (5.3) with an appropriate initial condition.

In a measurement evaluation the *inverse problem* is solved, where the electron density is to be calculated from the measured light profile $I(x)$. The classical solution of the inverse problem starts from the rate equation for the initial state ι of the observed transition, which is

$$d_x N_\iota = \sum_j \left[n_e(x) A_{\iota j}(x) + B_{\iota j} \right] N_j(x). \tag{5.6}$$

Using that the light profile $I(x)$ is proportional to N_ι, from Eq. (5.6) the electron density can be expressed as

$$n_e(x) = \frac{\frac{d}{dx}(\log I) - \sum_j \frac{N_j}{N_\iota} B_{\iota j}}{\sum_j \frac{N_j}{N_\iota} A_{\iota j}}. \tag{5.7}$$

Since the relative populations are not known *a priori*, Eq. (5.7) has to be solved simultaneously with the direct problem [68]. Note that this method does not require the absolute value of the N_ι population, only an arbitrarily normalized light profile.

For experimentally relevant plasma densities, there exists a point, where the collisional processes acting to populate and de-populate the ι level equalize, therefore the evolution of this population becomes independent of electron density (the measurement is insensitive in the vicinity of this point). Around this "blind point" the classical method is replaced by a technique, where the density is calculated as a fraction of integral quantities that are non-vanishing in the vicinity of the singular point [72]. This technique relies on the knowledge of the absolute N_ι profile, and the parameter $\alpha = N_\iota / I$ is found iteratively.

Recently, a Bayesian probabilistic method has been developed [31], based on the solution of the direct problem. The measured data are compared to direct calculations, and the most probable density profile is chosen. This approach requires much higher computational capacity, and often the constraint of monotonicity of the n_e profile. However, it is more stable than the previous techniques – even in the vicinity of the singular point – and allows for the evaluation of noisy data, accordingly, higher time resolution profile measurements. At the same time it provides the accuracy of the calculation in each point.

In paper F, we point out that neglecting the finite beam width, even for diagnostic beams, might cause non-negligible error in the calculated

density profile – regularly the underestimation of the pedestal density. We present a de-convolution based inversion algorithm, which, given the measured light profile, calculates the emission distribution along the beam axis, allowing for the use of conventional one-dimensional density reconstruction methods.

Chapter 6

Summary

In the present thesis theoretical and experimental aspects of collisional and turbulent transport in tokamaks are addressed.

In the first part of the thesis, the most important electrostatic drift wave instabilities driving the turbulent transport, the ion temperature gradient (ITG) and trapped electron (TE) modes, and the quasilinear fluxes driven by them are studied focusing on the effect of collisions.

In paper A, the collisionality dependence of quasilinear particle flux due to ITG and TE modes is investigated analytically. For weakly collisional plasmas, we derive the WKB solution of the trapped electron gyrokinetic equation, where the collisions are modeled by the Lorentz operator. In this model the frequencies and growth rates are considered as input parameters, therefore the dependences on different parameters – such as collisionality – through the eigenfrequency are neglected, and we use a simple, purely real model ballooning potential.

In accordance with previously published gyrokinetic simulation results, we find that, far from marginal stability, the inward flux due to ITG modes – caused mainly by magnetic curvature effects and thermodiffusion – is reversed as electron collisions are introduced. However, if the plasma is close to marginal stability, collisions might even enhance the inward particle transport. We compare the results calculated by using the Lorentz operator and an energy dependent Krook operator and conclude that the form of the collision operator determines the scaling with collisionality and therefore affects the collisionality threshold where the particle flow reverses. The difference between the two models is larger close to marginal stability. We find that, for low collisionalities, due to the boundary layer development of the non-adiabatic electron

distribution function at the trapped-passing boundary, the collisional contribution in the particle flux is proportional to the square root of the collisionality.

In paper B, we improved our "Collisional Model of Electrostatic Turbulence" (COMET) regarding several aspects and focus on the stability of the ITG mode and the ITG-driven quasilinear fluxes. Here, also the ion response is calculated in the long wavelength limit, and the mode frequencies are calculated from the quasineutrality constraint. We introduce a shear dependent imaginary part of the ballooning potential, which we motivate by a self-consistent variational solution of the ballooning eigenfunction problem. This is found to be important for the quantitatively accurate calculation of mode frequencies and fluxes. The improved model, where both the particle and energy fluxes are calculated, does not rely on the non-resonant expansion in magnetic drift frequencies.

We find that, although the frequencies and growth rates of ITG modes far from the stability threshold are only weakly sensitive to collisionality, the temperature gradient threshold for stability is significantly affected by electron-ion collisions for high enough logarithmic density gradients. The decrease of collisionality destabilizes the ITG mode driving an inward particle flux, which leads to the steepening of the density profile, in agreement with the trend found in experiments on the collisionality dependence of density peaking. Closed analytical expressions for the electron and ion perturbed density and temperature responses have been derived; and simple, but quite accurate algebraic approximations for these quantities are given.

In the next part of the thesis we focus on the collisional transport in transport barriers. In Paper C we calculate the neoclassical plateau regime transport in a tokamak pedestal. In tokamak pedestals with subsonic ion flows the radial scale of plasma profiles can be comparable to the ion poloidal Larmor radius, thereby making the radial electrostatic field so strong that the contribution of the $\mathbf{E} \times \mathbf{B}$ drift to the poloidal motion of ions can be comparable to the parallel streaming (mathematically, the normalized electric field $U = v_{\mathbf{E}\times\mathbf{B}} B / v_i B_p$ can be order unity). We calculate the modifications to neoclassical plateau regime adopting a novel kinetic approach allowing for short radial scale lengths and strong electric fields. We find that the ion heat diffusivity is reduced for large values of U, as the resonance causing plateau regime transport is shifted toward the tail of the distribution, but it is enhanced by almost 50%

if $U \approx 1$. Moreover, the poloidal ion and impurity flows are modified in the pedestal. The altered poloidal ion flow is most pronounced in the region of the strongest radial electric field where it modifies the friction of the electrons with the ions and can lead to an increase in the bootstrap current, by enhancing the coefficient of the ion temperature gradient term. We show that, unlike the banana regime, orbit squeezing does not affect the plateau regime results.

After the general and more analytical considerations we address more specific physics questions through gyrokinetic simulations based on measurements. In paper D we investigate the characteristics of microinstabilities in electron cyclotron heated (ECRH) and ohmic discharges in the T10 tokamak, aiming to find insights into the effect of auxiliary heating on the transport. Results from many different devices have shown that impurity accumulation can be reduced by central ECRH, while in some parameter regions ECRH does not affect the electron or impurity density profiles, or even peaking of these profiles is observed.

Trapped electron modes are found to be unstable in both the ohmic (OH) and the electron cyclotron (EC) heated scenarios studied. In the OH case the main drive is from the density gradient and in the EC case from the electron temperature gradient. The growth rates and particle fluxes exhibit qualitatively different scaling with the electron-to-ion temperature ratios in the two cases; in the OH case the electron particle flux decreases with this parameter, while it increases in the EC case. This is mainly due to the fact that the dominant drives and the collisionalities are different. Our linear gyrokinetic simulations indicate that the impurity convective flux is negative in both EC and OH cases, but it is significantly lower in the EC case. Furthermore the impurity diffusion coefficient is lower in that case. As a consequence, the impurity peaking factor is lower in the EC; a trend that is consistent with the observations, however according to the simulations it does not change sign when electron cyclotron heating is applied. A sign change in the peaking factor is, therefore probably due to some additional physical mechanism, such as poloidal asymmetry of the impurity ions, not accounted for in the linear gyrokinetic simulations.

In paper E the effect of primary ion species of differing charge and mass – specifically, deuterium, hydrogen and helium – on instabilities and transport is studied in DIII-D plasmas through gyrokinetic simulations with GYRO. The main motivation of this paper is the "isotope scaling problem": the experimentally observed favorable scaling of the

energy confinement time with isotope mass is in conflict with the gyro-Bohm scaling. In linear simulations under imposed similarity of the profiles there is an isomorphism between the linear growth rates of hydrogen isotopes, but the growth rates are higher for $Z > 1$ main ions due to the appearance of the charge in the Poisson equation. On ion scales the most significant effect of the different electron-to-ion mass ratio appears through collisions stabilizing trapped electron modes. In nonlinear simulations significant favorable deviations from pure gyro-Bohm scaling are found due to electron-to-ion mass ratio effects and collisions. The presence of any non-trace impurity species cannot be neglected in a comprehensive simulation of the transport; including carbon impurity in the simulations caused a dramatic reduction of energy fluxes. The transport in the analyzed deuterium and helium discharges could be well reproduced in gyrokinetic and gyrofluid simulations while the energy transport in the hydrogen discharge was much higher than the gyrokinetic predictions taking neoclassical flows into account. This significant discrepancy is the subject of ongoing investigation and should be a basis of future validation efforts.

Finally the thesis touches upon a purely experimental problem; the magnitude and characteristics of the error in alkali beam emission spectroscopy (BES) density profile measurements due to finite beam width are analyzed and a deconvolution based correction algorithm is introduced. If the line of sight is far from tangential to the flux surfaces and the beam width is comparable to the scale length of the light profile, the observation might cause an undesired smoothing of the light profile, resulting in the underestimation of the measured electron density. In paper F, the characteristics and magnitude of this systematic error is studied; a general estimation of the maximal relative error is presented depending on plasma parameters and observation geometry. We demonstrate a deconvolution based correction method by its application in simulated BES measurements of the COMPASS and TEXTOR tokamaks. The method gives a good estimate of the emissivity along the beam line from the measured light profile so that the level of the remaining error in the calculated density after correction is in the order of the accuracy of the density profile calculation algorithm. The method allows the use of the conventional one dimensional density calculation algorithms even for configurations, where the finite beam width is not negligible.

References

[1] J. W. Milnor, Topology from the Differentiable Viewpoint, *University of Virginia Press* (1965).

[2] L. Spitzer, Phys. Fluids **1**, 253-254 (1958).

[3] J. A. Wesson, Tokamaks, *Oxford University Press* (2004).

[4] M. Greenwald, J. Terry, S. Wolfe, S. Ejima, M. Bell, S. Kaye, and G. H. Neilsen, Nucl. Fusion **28**, 2199 (1988).

[5] J. Wesson, The science of JET (JET Joint Undertaking, Abingdon, Oxon, 2000), JET-R(99)13.

[6] Progress in the ITER physics basis, Nucl. Fusion **47**, S1 (2007).

[7] ITER Physics basis, Nucl. Fusion **39**, 2175 (1999).

[8] J. Weiland, Collective modes in inhomogeneous plasma, *IOP Bristol*, (2000).

[9] T. H. Dupree and D. J. Tetreault, Phys. Fluids **21**, 425 (1978).

[10] A. Casati, C. Bourdelle, X. Garbet, F. Imbeaux, J. Candy, F. Clairet, G. Dif-Pradalier, G. Falchetto, T. Gerbaud, V. Grandgirard, O.D. Gurcan, P. Hennequin, J. Kinsey, M. Ottaviani , R. Sabot, Y. Sarazin, L. Vermare, and R.E. Waltz, Nucl. Fusion **49**, 085012 (2009).

[11] A. A. Galeev, V. N. Oraevskii, and R. Z. Sagdeev, Soviet Physics JETP **17**, 615 (1963).

[12] W. Horton, D. Choi, and W. M. Tang, Phys. Fluids **24**, 1077 (1981).

[13] S. C. Guo, and F. Romanelli, Phys. Fluids **B5**, 520 (1993).

[14] H. Biglari, P. H. Diamond, and M. N. Rosenbluth, Phys. Fluids **B1**, 109 (1989).

[15] W. M. Manheimer, K. R. Chu, E. Ott, and J. P. Boris, Phys. Rev. Lett. **37**, 286 (1976).

[16] J. W. Connor, R. J. Hastie, and P. Helander, Plasma Phys. Control. Fusion **48**, 885 (2006).

[17] Y. C. Lee, J. Q. Dong, P. N. Guzdar, and C. S. Liu, Phys. Fluids **30**, 1331 (1987).

[18] F. Jenko, J. Plasma Fusion Res. SERIES **6**, 11 (2004).

[19] W. Guttenfelder, J. Candy, S. M. Kaye, W. M. Nevins, E. Wang, R. E. Bell, G. W. Hammett, B. P. LeBlanc, D. R. Mikkelsen, and H. Yuh, Phys. Rev. Lett. **106**, 155004 (2011).

[20] R. D. Stambaugh, S. M. Wolfe, R. J. Hawryluk, J. H. Harris, H. Biglari, S. C. Prager, R. J. Goldston, R. J. Fonck, T. Ohkawa, B. G. Logan, and E. Oktay, Phys. Fluids **B2**, 2941 (1990).

[21] J.W. Connor, T. Fukuda, X. Garbet, C. Gormezano, V. Mukhovatov, M. Wakatani, the ITB Database Group, the ITPA Topical Group on Transport and Internal Barrier Physics, Nucl. Fusion **44**, R1 (2004).

[22] ASDEX Team, Nucl. Fusion **29**, 1959 (1989).

[23] P.B. Snyder, N. Aiba, M. Beurskens, R.J. Groebner, L.D. Horton, A.E. Hubbard, J.W. Hughes, G.T.A. Huysmans, Y. Kamada, A. Kirk, C. Konz, A.W. Leonard, J. Lönnroth, C.F. Maggi, R. Maingi, T.H. Osborne, N. Oyama, A. Pankin, S. Saarelma, G. Saibene, J.L. Terry, H. Urano, and H.R. Wilson, Nucl. Fusion **49**, 085035 (2009).

[24] K. McCormick, S. Fiedler, G. Kocsis, J. Schweinzer, and S. Zoletnik, Fus. Eng. and Des. **34-35**, 125 (1997).

[25] S. Zoletnik, M. Anton, M. Endler, S. Fiedler, M. Hirsch, K. McCormick, and J. Schweinzer, Phys. Plasmas **6**, 4239 (1999).

[26] N. Winsor, J.L. Johnson, and J.M. Dawson, Phys. Fluids **11**, 2448 (1968).

[27] P. Helander, and D. J. Sigmar, Collisional Transport in Magnetized Plasmas, *Cambridge University Press* (2002).

[28] F. L. Hinton, and R. D. Hazeltine, Rev. Mod. Phys. **48**, 239 (1976).

[29] P. J. Catto, I. B. Bernstein, and M. Tessarotto, Phys. Fluids **30**, 2784 (1987).

[30] G. Kagan and P. J. Catto, Plasma Phys. Control. Fusion **52**, 055004 (2010).

[31] R. Fischer, E. Wolfrum, J. Schweinzer and the ASDEX Upgrade Team, Plasma Phys. Control. Fusion **50**, 085009 (2008).

[32] W. Horton, Rev. Mod. Phys. **71**, 735 (1999).

[33] J. W. Connor, and O. P. Pogutse, Plasma Phys. Control. Fusion **43**, 155 (2001).

[34] H. Sugama and W. Horton, Phys. Plasmas **5**, 2560 (1998).

[35] J. Candy and E. Belli, General Atomics Technical Report **GA-A26818** (2010).

[36] J. W. Connor, R. J. Hastie, and J. B. Taylor, Plasma Physics **22**, 757 (1980).

[37] J. Candy, R. E. Waltz, and M. N. Rosenbluth, Phys. Plasmas **11**, 1879 (2004).

[38] T. Dannert and F. Jenko, Phys. Plasmas **12**, 072309 (2005).

[39] F. Romanelli and S. Briguglio, Phys. Fluids **B2**, 754 (1990).

[40] W. M. Tang, Nucl. Fusion **18**, (1978).

[41] J. W. Connor, and H. R. Wilson, Plasma Phys. Control. Fusion **36**, 719 (1994).

[42] B. B. Kadomtsev, and O. P. Pogutse, Review of Plasma Physics, ed. M. A. Leontovich, *Consultants Bureau, New York*, (1970) Vol. 5, p. 249.

[43] F. Romanelli, Phys. Fluids **B1**, 1018 (1989).

[44] C. Estrada-Mila, J. Candy, and R. E. Waltz, Phys. Plasmas **12**, 022305 (2005).

[45] M. Ottaviani, W. Horton, and M. Erba, Plasma Phys. Control. Fusion **39**, 1461 (1997).

[46] L. Bai, X. M. Qiu, L. Huang, and X. M. Song, Phys. Plasmas **3**, 3004 (1996).

[47] P. H. Diamond, S.-I. Itoh, K. Itoh, and T. S. Hahm, Plasma Phys. Control. Fusion **47**, R35 (2005).

[48] T. S. Hahm, and K. H. Burrell, Phys. Plasmas **2**, 1648 (1995).

[49] B. B. Kadomtsev, and O. P. Pogutse, Sov. Phys. Dokl. **14**, 470 (1969).

[50] B. A. Trubnikov, Review of Plasma Physics, ed. M. A. Leontovich, *Consultants Bureau, New York*, (1965) Vol. 1, p. 105.

[51] L. D. Landau, Physikalische Zeitschrift der Sowjetunion **10**, 154 (1936).

[52] S. P. Hirshman and D. J. Sigmar, Phys. Fluids **19**, 1535 (1976).

[53] C. Angioni, A. G. Peeters, G. V. Pereverzev, F. Ryter, G. Tardini, and the ASDEX Upgrade Team, Phys. Rev. Lett. **90**, 205003 (2003).

[54] A. A. Ware, Phys. Rev. Lett. **25**, 15 (1970).

[55] H. Weisen, A. Zabolotsky, C. Angioni, I. Furno, X. Garbet, C. Giroud, H. Leggate, P. Mantica, D. Mazon, J. Weiland, L. Zabeo, K. D. Zastrow, and JET-EFDA Contributors, Nucl. Fusion **45**, L1 (2005).

[56] M. Greenwald, C. Angioni, J. W. Hughes, J. Terry, and H. Weisen, Nucl. Fusion **47**, L26 (2007).

[57] H. Takenaga, K. Tanaka, K. Muraoka, H. Urano, N. Oyama, Y. Kamada, M. Yokoyama, H. Yamada, T. Tokuzawa, and I. Yamada, Nucl. Fusion **48**, 075004 (2008).

[58] B. Coppi and C. Spight, Phys. Rev. Lett. **41**, 551 (1978).

[59] C. Angioni, A. P. Peeters, F. Jenko, and T. Dannert, Phys. Plasmas **12**, 112310 (2005).

[60] P. Mantica, D. Strintzi, T. Tala, C. Giroud, T. Johnson, H. Leggate, E. Lerche, T. Loarer, A. G. Peeters, A. Salmi, S. Sharapov, D. Van Eester, P. C. de Vries, L. Zabeo, and K.-D. Zastrow, Phys. Rev. Lett. **102**, 175002 (2009).

[61] J. Candy, C. Holland, R.E. Waltz, M.R. Fahey, and E. Belli, Phys. Plasmas **16**, 060704 (2009).

[62] G. Staebler and J. Kinsey, Phys. Plasmas **17**, 122309 (2010).

[63] I. H. Hutchinson, Principles of Plasma Diagnostics; *Cambridge University Press* (2002).

[64] B. Scweer, Fus. Sci. Technol. **49**, 404 (2006).

[65] G. R. McKee, C. Fenzi, R. J. Fonck, and M. Jakubowski, Rev. Sci. Instrum. **74**, 2014-2019 (2003).

[66] R. J. Fonck, P. A. Duperrex, and S. F. Paul, Rev. Sci. Instrum. **61**, 3487 (1990).

[67] S. Zoletnik, G. Petravich, A. Bence, M. Berta, S. Fiedler, K. McCormick, and J. Schweinzer, Rev. Sci. Instrum. **76**, 073504 (2005).

[68] Z. A. Pietrzyk, P. Breger, and D. D. R. Summers, Plasma Phys. Control. Fusion **35**, 1725-1744 (1993).

[69] S. Zoletnik, M. Anton, M. Endler, S. Fiedler, M. Hirsch, K. McCormick, and J. Schweinzer, Phys. Plasmas **6**, 4239 (1999).

[70] R. Brandenburg, J. Schweinzer, S. Fiedler, F. Aumayr, and H. P. Winter, Plasma Phys. Control. Fusion **41**, 471 (1999).

[71] K. McCormick, S. Fiedler, G. Kocsis, J. Schweinzer, and S. Zoletnik, Fus. Eng. Des. **34-35**, 125 (1997).

[72] J. Schweinzer, E. Wolfrum, F. Aumayr, M. Pöckl, H. Winter, and A. Unterreiter, Plasma Phys. Control. Fusion **34**, 1173 (1992).

[73] R. P. Schorn, E. Hintz, D. Rusbüldt, F. Aumayr, M. Schneider, E. Unterreiter, and H. Winter, Applied Physics B **52**, 71 (1991).

[74] S. Zoletnik, S. Fiedler, G. Kocsis, G. K. McCormick, J. Schweinzer, and H. P. Winter, Plasma Phys. Control. Fusion **40**, 1399 (1998).

Included papers A-F

Paper A

T. Fülöp, I. Pusztai and P. Helander, "Collisionality dependence of the quasilinear flux due to microinstabilities", Phys. Plasmas **15**, 072308 (2008).

Paper B

I. Pusztai, T. Fülöp, J. Candy and R. J. Hastie, "Collisional model of quasilinear transport driven by toroidal electrostatic ion temperature gradient modes", Phys. Plasmas **16**, 072307 (2009).

Paper C

I. Pusztai and P. J. Catto, "Neoclassical plateau regime transport in a tokamak pedestal", Plasma Phys. Control. Fusion **52**, 075016 (2010).

Paper D

I. Pusztai, S. Moradi, T. Fülöp, and N. Timchenko, "Characteristics of microinstabilities in electron cyclotron and ohmic heated discharges", Phys. Plasmas. **18**, 082506 (2011).

Paper E

I. Pusztai, J. Candy, and P. Gohil, "Isotope mass and charge effects in tokamak plasmas", accepted for publication in Phys. Plasmas.

Paper F

I. Pusztai, G. Pokol, D. Dunai, D. Réfy, G. Pór, G. Anda, S. Zoletnik and J. Schweinzer, "Deconvolution-based correction of alkali beam emission spectroscopy density profile measurements", Rev. Sci. Instrum. **80**, 083502 (2009).